이학박사학위논문

Microwave field enhancement by deep subwavelength metallic gaps down to five nanometers

5 나노미터에 이르는 파장 이하 금속 틈에 의한 마이크로파의 집속

2017년 2월

서울대학교 대학원
물리천문학부

이 광 희

Microwave field enhancement by deep subwavelength metallic gaps down to five nanometers

지도교수 김 대 식

이 논문을 이학박사학위논문으로 제출함
2017년 2월

서울대학교 대학원
물리천문학부
이 광 희

이광희의 박사학위논문을 인준함
2017년 2월

위 원 장 박 건 식 (인)
부위원장 김 대 식 (인)
위 원 최 석 봉 (인)
위 원 박 철 환 (인)
위 원 김 성 환 (인)

Abstract

In this dissertation, I describe experimental demonstrations of strong field enhancements in microwave regime achieved by deep subwavelength metallic gaps down to 5 nanometers. I built a Ku band (12~18 GHz) free-space setup to measure transmittances and electric field enhancement factors of the samples. I prepared λ/400-width slot antennas by punching aluminum foils with a razor blade and the hand-made antennas exhibited good agreements to the previous studies of terahertz nanoantennas which have a similar aspect ratio of the incident wavelength and the widths of slots. To investigate deeper subwavelength regime, λ/10,000,000-width nanogaps were fabricated by high-throughput atomic layer lithography. I built three open-ended waveguide pair setups to cover Ku, K (18~26.5 GHz), and Ka (26.5~40 GHz) band spectra and observed giant electric field enhancement factors up to 5,000 with the nanogaps. I also performed terahertz time-domain spectroscopy with the same sample and confirmed a convergence to the microwave range. As a potential application of subwavelength microwave optics, I exhibited a λ/2,000-width microwave switch based on insulator-metal transition. The aforementioned researches would open up a way to enhance nonlinearities and detection sensitivities of microwave and millimeter-wave optics applications and enable non-invasive molecule trappings and designed fluidic controls by light.

Keyword : microwave transmission, field enhancement, sub-wavelength optics, nanogap, terahertz time-domain spectroscopy

Student Number : 2012-30106

Table of Contents

List of Figures

Chapter 1. Introduction

Electromagnetic wave confinement into subwavelength metallic structures has been intensely studied in the broad range of geometries and frequencies.[1-6] Recently, light confinement has been achieved at a few nanometers-wide apertures[7-9] and even at an Ångstrom scale.[10, 11] Such strong confinement of electromagnetic wave enables not only improved applications e.g. surface-enhanced Raman scattering sensors,[12, 13] molecule detectors for small quantities,[14] and insulator-to-metal phase transition metamaterials utilizing vanadium dioxide (VO_2) thin film[15, 16] but also novel observations of boosted multiphoton processes,[17, 18] non-local effects,[19] Fowler-Nordheim tunneling,[20] terahertz quantum plasmonics at the supernanometer regime,[21] etc. In principle, the squeezing of electromagnetic waves onto subwavelength metallic structures can be achieved at arbitrary frequency and length scales. However, at longer wavelength regimes i.e. microwave and radio frequencies, degree of wave confinement has been limited to micron scale apertures.[22-25] Although there have been microwave studies concerned with nanoscale such as nanomaterial characterization,[26] near-field probing,[27] and superconducting circuitry,[28] these works are not in the context of electromagnetic wave confinement. The main reason which hinders further studies of microwave confinement is a lack of a fabrication method satisfying both nanometer-scale feature size and millimeter-scale pattern size. Despite electron-beam or focused-ion-beam lithography can be utilized to fabricate few-millimeter-long nanostructures, such serial writing

techniques are time-consuming and cost-ineffective.

In this dissertation, I demonstrate extreme squeezing of microwave into deep subwavelength metallic gaps to push the limit of the light confinement towards the lower frequency regime. The structures used in this work are metallic slot antennas with fundamental resonance lengths and deep subwavelength widths. According to the widths of the gaps, the samples were fabricated with various methods e.g. perforation by a razor blade, photolithography, focused ion beam (FIB), and atomic layer lithography.[8, 9, 29] Notably, the atomic layer lithography is free from the trade-off between resolution and pattern size, found in most of top-down lithography techniques, thus enables atomic-scale resolution of width while maintaining enough length for a resonant microwave transmission. Details of the fabrication methods mentioned above will be stated in chapter 2.

To measure microwave transmittances of the subwavelength gaps, I built a horn antenna pair and open-ended waveguide pair setups mainly operating in Ku band (12~18 GHz), additionally in K band (18~26.5 GHz) and Ka band (26.5~40 GHz). Waveguide components were combined with a microscope and amplifiers while microwave trapping experiments. Each setup was selectively connected to a vector network analyzer (VNA) for its unique purpose and calibrated with thru-reflect-line standard[30, 31] before measurement. To span upper limit of measurement frequency up to 1 THz, home-built terahertz time-domain spectroscopy (THz-TDS) setup was also used. Details of the setups will be explained in chapter 3.

With the subwavelength metallic gaps and the experimental setups described above, I measured transmittances of the sample and deduced electric field enhancement factors from Kirchoff integral formalism.[32]

At first, I will discuss about the microwave field enhancement by λ/400-width gaps, studied with 50-μm-wide hand-made gaps and horn antenna pair setup, in chapter 4. Since the wavelength-to-width ratio was in similar regime of terahertz waves and nanoantennas,[14, 32-37] the field enhancement factors and coupling characteristics between adjacent antennas showed good quantitative agreements. In chapter 5, experimental results of much deeper subwavelength regime, up to nanometer-scale, will be given. I approached to the λ/10,000,000-scale funneling of waves with the samples made by atomic layer lithography and the transmission setups that covers 12 GHz~1 THz frequency range.

In chapter 6, I will conclude this dissertation with a summary and a brief introduction of potential applications of the microwave field enhancement: insulator-to-metal transition based switching device.

Chapter 2. Preparation of subwavelength gaps

It is important to choose the sample fabrication process for the desired regime of field confinement, i.e. wavelength-to-width aspect ratio. In this chapter, I will introduce four fabrication methods to prepare subwavelength metallic gaps with various widths used in this dissertation. The methods are as follows: perforation by razor blade, photolithography, FIB, and atomic layer lithography. Each method has the pros and cons of fabrication time and cost, minimum resolution, maximum pattern size, yield, rigidity, etc. thus one should consider the experimental conditions to select an appropriate fabrication technique.

2.1. Perforation by razor blade

At first, I will describe about the perforation by razor blade. This method is the simplest yet a powerful way to fabricate negative patterns of deep subwavelength feature sizes, especially for microwave range, without high cost facilities and clean room. In this work, aluminum foils of 17 μm thickness were perforated, rather than cut, by a piece of razor blade since cutting by a blade may cause human error of slot length, a very critical parameter that affects resonance frequency. Before perforation, aluminum foils were attached to foam board substrates using adhesive spray for rigidity of the sample and easier handling. Refractive index of foam board in microwave range is about 1.03, nearly unity, thus foam board is free from substrate effects such as red shift of resonance frequencies and multiple reflection.[33, 38, 39] The razor blade was cut to be the half of the center wavelength of measurable spectrum. Since Ku band (12~18 GHz) horn antennas will be used for transmittance measurements, the half of the center wavelength is 1 cm. But after perforation, resultant length of the slot is slightly longer than that of the piece of blade. Therefore, it is recommended to make a test sample with various pieces of blade until the desired resonance frequency is found.

Figure 2.1 (a) is a photograph of perforated aluminum foils on foam boards. Since the beam size of incident wave is 5 cm x 5 cm (details are in chapter 3.1), the size of patterning area and the samples were determined as 6 cm x 6 cm and 10 cm x 10 cm, respectively. Figure 2.1 (b) ((c)) is a top view (cross sectional) microscope image of the slot. As shown in (b), the gap width is about 50 μm, corresponding to λ/400.

This wavelength-to-width ratio is similar to that of nanoslot antennas operating in terahertz range.[33-35, 37] However as shown in (c), the metal in the slot area is not blown away but forms slanted or tapered gap geometry unlike using other lithography techniques or FIB milling. Thus an effective width should be defined to experimentally estimate field enhancement factors and compare with theoretical results based on ideal slot geometry. Details will be discussed in chapter 4.3. Meanwhile, the slanted or tapered geometry shows a potential of very narrow gaps regardless of the thickness of the blade. By careful control of perforating force, a deeper subwavelength metallic gaps may be fabricated.

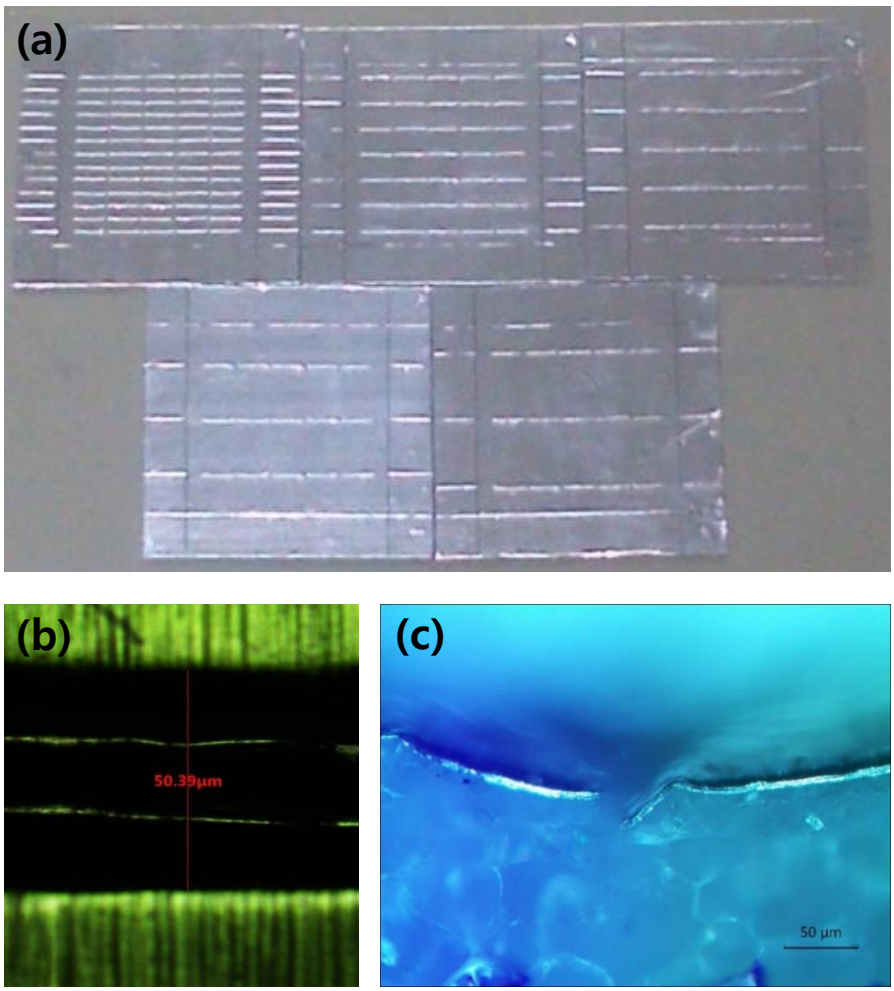

Figure 2.1 Images of fabricated hand-made slot antennas by perforation of aluminum foil. (a) Photograph of perforated slots. Dimensions of the patterned area and the entire sample are 6 cm x 6 cm and 10 cm x 10 cm, respectively. Slot length is 1 cm and periods are 5, 10, 15, 20, 25 mm in vertical direction and 12 mm in horizontal direction. (b) Top view microscope image of the slot. (c) Cross sectional microscope image of the slot.

2.2. Photolithography

Second method for sample preparation is photolithography. Laboratory scale photolithography can fabricate well defined patterns over whole wafer area with resolution of few micrometers. This technique easily provides a deeper subwavelength metallic gaps of 10 μm width, corresponding to λ/2,000 when the center wavelength is 2 cm. On the other hand, it is needed to prepare an additional photomask and hard to fabricate nanoscale patterns without special techniques such as phase-shift mask[40], immersion lithography[41, 42] and double patterning lithography.[43]

The λ/2,000-scale samples used in this work were fabricated by standard photolithography process with image reversal as follows.[44] At first, an undoped silicon substrate (500-μm-thick, 1,000 Ω·cm) was cleansed by sonication while immersed in acetone and isopropyl alcohol (IPA) for each 5 min. After drying with nitrogen gas, commercially available photoresist (AZ 5214E, AZ Electronic Materials) was spin-coated at 4,000 rpm onto the substrate for 60 s, followed by 60 s soft bake at 90 ℃. Then the photoresist film was made in contact with a photomask of the desired microstructure (in most cases, arrays of 4-mm-long and 10-μm-wide slots with few millimeters periodicity), and exposed to ultraviolet light of 30 mW/cm^2 intensity for 7 s using I-line mask aligner (Karl Süss MJB-3, Süss Microtec). After that, the photoresist and the substrate was baked at 115 ℃ for 75 s. Then the photoresist was exposed to ultraviolet light of 30 mW/cm^2 intensity again for 15 s without photomask for an image reversal process. Finally, patterns were developed by AZ 500 MIF developer (AZ Electronic

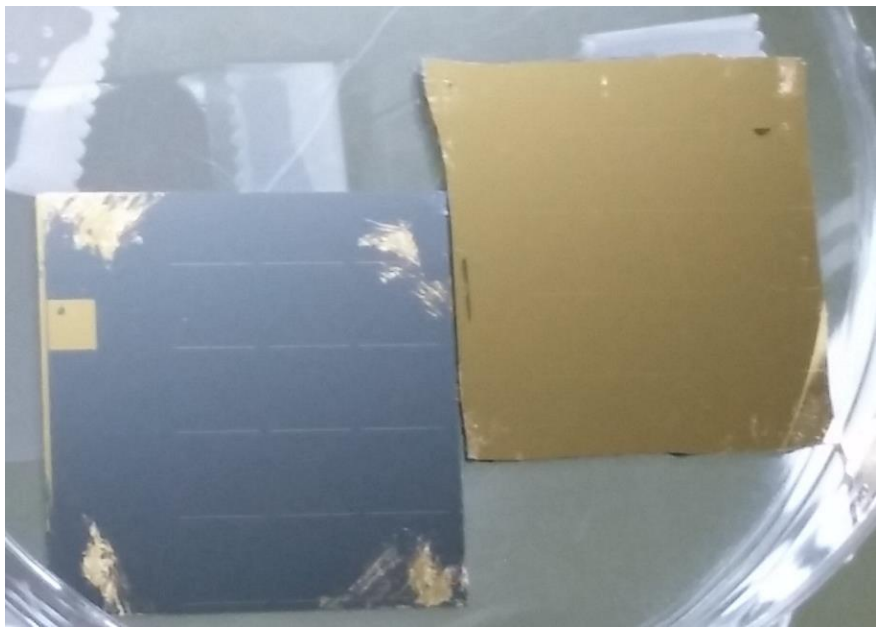

Figure 2. 2 Photograph of (left) positive and (right) negative subwavelength antennas fabricated by photolithography. 3 nm Cr and 97 nm Au layers were patterned on undoped Si substrate. Length is 4 mm and width is 10 μm for antennas of both samples.

Materials) for 45 s, cleansed by deionized water, and dried in nitrogen gas; when necessary, we repeated the process with 10~15 s developing time. After the photolithography processes, 3-nm-thick chromium as an adhesive layer and 97-nm-thick gold layer were deposited on patterned resist arrays using electron beam evaporator (KVE-E2000, Korea Vacuum Tech). Deposition rate was changed to be 0.1 Å/s at the beginning for quality roughness, 1 Å/s for reducing deposition time, and 0.1 Å/s for the fine finishing. After the deposition, the photoresist was removed by immersing in acetone and the sample was cleaned by deionized water and dried by nitrogen gas. Finally, only the predesigned metallic antenna arrays were left as shown in Figure 2.2.

When the substrate is transparent, the photolithography process needs modifications to obtain a quality pattern with good verticality.

For instance, the procedure may be changed with 1-mm-thick slide glass substrate as follow. At first, the substrate was cleansed with the same condition of Si substrate. Then the metallic layers were deposited before spin coating of photo resist. Hexamethyldisilazane (HMDS) was spin-coated at 4,000 rpm for 60 s, followed by 60 s soft bake at 90 ℃. Commercially available photoresist (AZ 5214E, AZ Electronic Materials) was also spin-coated and baked with the same condition. Then the sample was made in contact with a photomask and exposed to ultraviolet light of 10 mW/cm^2 intensity for 10 s using mask aligner (Midas aligner, Midas System Co., Ltd). Without image reversal process, patterns were developed by AZ 300 MIF developer (AZ Electronic Materials) for 25 s, cleansed by deionized water, and dried in nitrogen gas; if necessary, the process can be repeated with shorter developing time. After the photolithography process, the sample was milled by argon ions (80 V acceleration voltage and 1.7 mA beam current) with normal incidence for 5 min while rotating (KVET-IM2000L, Korea Vacuum Tech). The milled sample was rinsed with acetone and IPA in sequence and dried with nitrogen gas to remove residues. Following the above procedure, the desired metallic gaps were patterned as shown in Figure 2.3.

Figure 2. 3 Photograph of (left) positive and (right) negative subwavelength antennas on slide glass substrate. 3 nm Cr and 97 nm Ag layers were patterned by photolithography. Length is 4 mm and widths are 5, 10, 20, 50 μm for antennas of both samples.

2.3. Focused ion beam

Third method for sample fabrication is focused ion beam (FIB) milling. FIB milling is a serial writing technique using physical etching due to the collision of accelerated ions (Ga^+ ions in most cases) and the target material. This method offers a nanoscale resolution down to few tens of nanometers (even few nanometers with helium ions) and does not need a patterning mask unlike photolithography. Instead, it would take very long time to write nanoscale patterns over large area. FIB milling has been widely used to fabricate samples for nano-optics[45-47] and a number of metallic nanogaps operating in THz range were also fabricated by this method.[14, 33, 36, 39]

In this work, a 2 x 10 array of nano-slot was formed in 100-nm-thick metal film (3 nm chromium and 97 nm gold) thermally evaporated on undoped silicon substrate (500-μm-thick, 1,000 Ω·cm), by stitching of dual-beam FIB (FIB200, FEI) milling. As shown in Figure 2.3, width and length of the nano-slots were 300 nm and 3.5 mm, respectively. It is noted that the fabrication time was nearly a month since the milling rate was about 1 slot / 5 hr. Because of this long working time, electron beam lithography, having a similar resolution compared to FIB, cannot be used to fabricate the sample in this work due to degradation of electron beam resist.

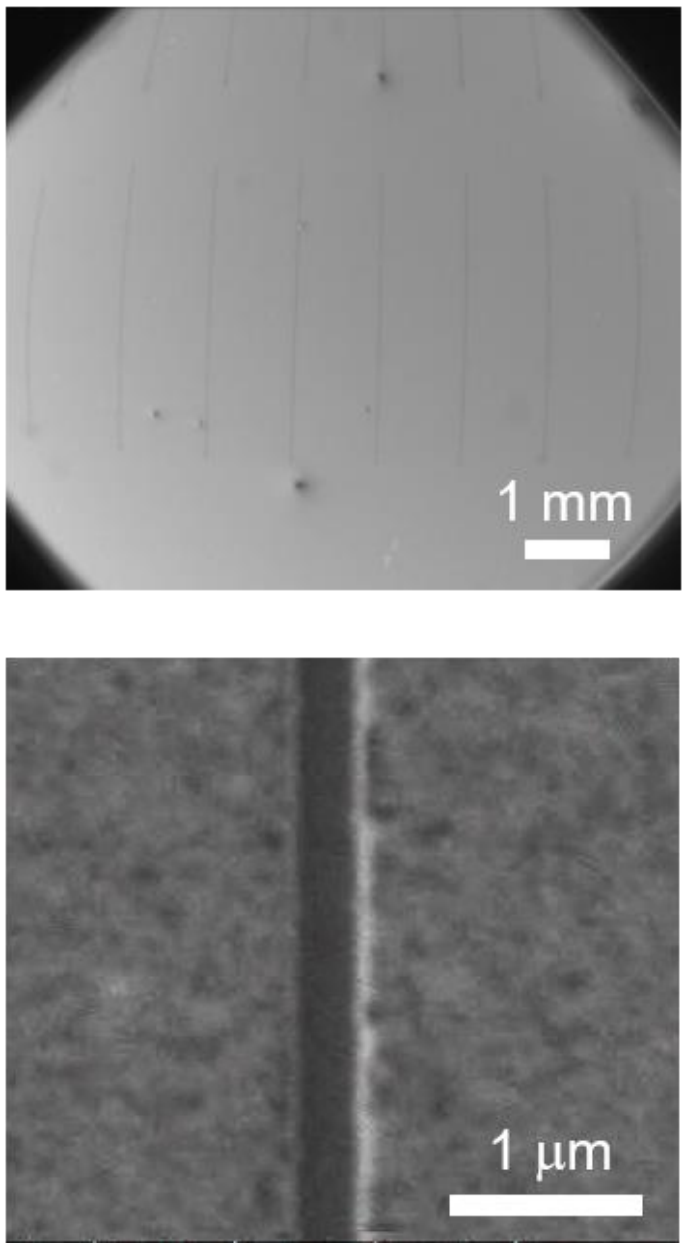

Figure 2. 4 Top view scanning electron microscope images of 100-nm-thick slot antennas on undoped Si fabricated by FIB milling. Before milling, 3-nm-thick Cr and 97-nm-thick Au layers were deposited on undoped Si substrate. (Top) mm-scale view. Length of each slot is 3.5 mm and distance between adjacent slots is 1 mm in both vertical and horizontal direction. (Bottom) Enlarged view. Width of each slot is 300 nm.

2.4. Atomic layer lithography

The last fabrication method of this chapter is the modified high-throughput atomic layer lithography.[29] The atomic layer lithography utilizes atomic layer deposition for conformal dielectric spacer coating onto metallic pre-patterns (1st layer). And metal is deposited again to fill inside the coated 1st metallic layer. After removal of excessive 2nd metal on the 1st layer, the metal-dielectric-metal gaps is revealed. The width of the gaps is defined by the thickness of atomic layer deposition and the size of the gaps is decided by pre-patterning using photolithography[8, 9, 29] or electron beam lithography.[48] Since the width and the size is determined separately by two techniques, the atomic layer lithography is free from the trade-off between resolution and pattern size, found in most of top-down lithography techniques, and is able to achieve atomic-scale resolution of width while maintaining enough length for a resonant microwave transmission, as mentioned in chapter 1. The original atomic layer lithography used an adhesive tape to mechanically peel off the excessive metal.[8] However this may cause low yield and fragile patterns since the 2nd metal layer should be deposited without adhesion layer for exfoliation by adhesive tape. Due to the large beam size of incident microwave, over 1 cm^2, and contact of the sample and waveguide (details will be discussed in chapter 3.2), high yield and rigidity of the sample is mandatory for the microwave experiments.

In this work, the modified atomic layer lithography with sacrificial layer deposition and chemical etching[29] was adopted to ensure high-throughput fabrication. Unlike the taping method used to peel off the

excess metal, chemical etching can be performed under well-defined and uniform conditions and thus provides high-throughput fabrication. Moreover, the fabricated nanogaps are highly rigid since both metallic regions surrounding the spacer are deposited with adhesion layer. Figure 2.4 shows the flow of the modified atomic layer lithography process. At first, 3-nm-thick chromium as an adhesion layer and 97-nm-thick gold were deposited on the undoped silicon substrate (500-μm-thick, 1,000 Ω·cm) by thermal evaporator. Then 150-nm-thick aluminum and 30-nm-thick chromium sacrificial layer were patterned by standard photolithography, as described in chapter 2.3 (AZ5214E, image reversal). The patterned sample was milled by Ar ions (0.5 nm/min etching rate, 5 minutes for the top and 5 minutes for the sidewall) to form outer region of the nanogap rings. The alumina (Al_2O_3) spacer layer is then coated by atomic layer deposition (1.1 Å/cycle at 250 ℃). After coating the spacer, chromium and gold are deposited again to fill inside the rings and the gaps are exposed by chemical etching of aluminum (KOH, 45%) and chromium (CR-7, Cyantek).

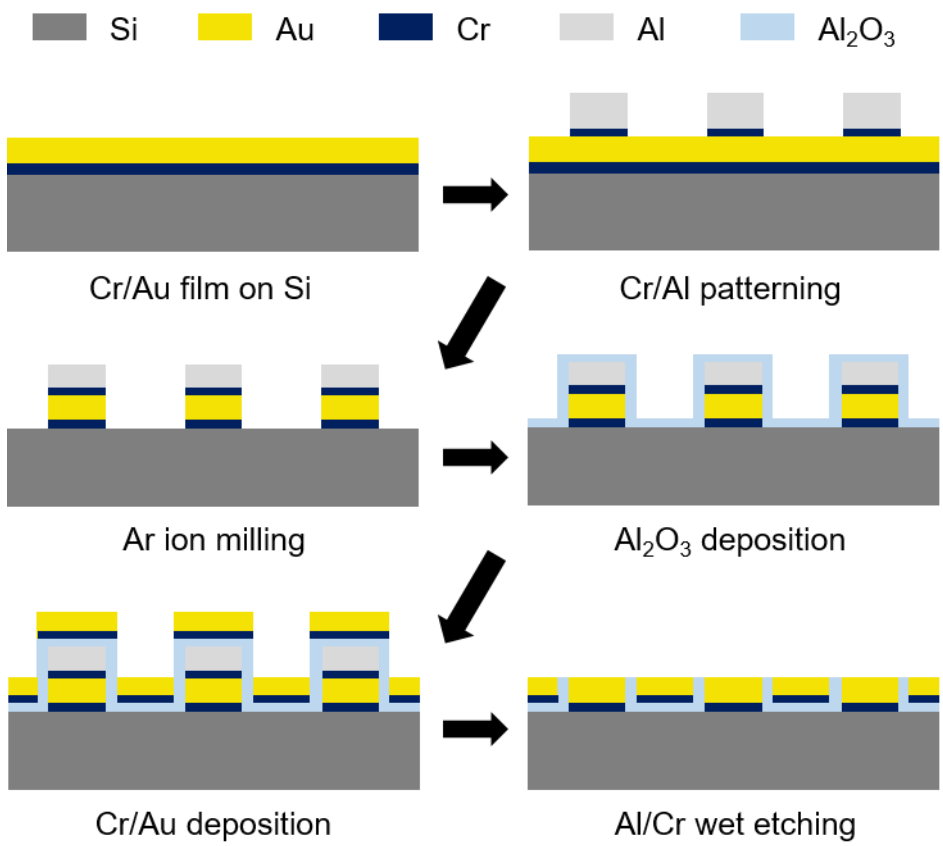

Figure 2. 5 Schematics of atomic layer lithography process containing metal deposition, ion milling, atomic layer deposition, and chemical etching.

Chapter 3. Experimental setups

In this chapter, I will describe experimental setups used in this dissertation. I built three kinds of microwave setups: horn antenna pair in anechoic chamber, three pairs of open-ended waveguide, and high power waveguide combined with microscope. Each setup has its unique purpose and was selectively connected to vector network analyzer (VNA) while using. I will also introduce a homebuilt terahertz time-domain spectroscopy (THz-TDS) setup which expands transmittance spectra up to more than 1 THz.

3.1. Horn antenna pair

In this section, I will describe about horn antenna pair for free-space transmittance measurement as shown in Figure 3.1. This setup is useful to measure transmittances of relatively large samples up to few centimeters or more i.e. λ/400-width hand-made gaps. Here is the process of making the setup. At first, an anechoic chamber was made of pyramidal microwave absorbers with 4-inch height (KSS-4, Korea Shield System, Ltd). The absorbers were attached to acryl plates using adhesive spray and supported by aluminum profiles. At the center of anechoic chamber, a metallic 6 cm x 6 cm aperture sandwiched by two absorbing 5 cm x 5 cm apertures, made by removing a single pyramid in the center of pyramidal absorber arrays, was arranged. As a result, the chamber has two absorbing cells sharing a 5 cm x 5 cm square hole. The metallic aperture serves as a sample mount and blocks side lobes of transmitting antenna and scattered waves from surroundings. The absorbing apertures minimize multiple reflections due to the metallic aperture and trim incident waves to be approximately plane waves. Inside each cell, a 20 dB standard gain Ku band horn antennas (SGA-150, Seavey Engineering Associates, Inc) or 7.5~18 GHz multi octave horn antenna (LB-75180-20, Chengdu AINFO inc.) was placed. The two types of horn antenna showed similar performances in Ku band. Distances between absorbing walls and the horn antenna were more than 20 cm, ten times of the center wavelength of Ku band. Although the distances don't correspond to far field region but radiating near field range,[49, 50] the distances were enough to avoid reactive near field interactions while measuring transmittances of the hand-made gap

samples. All the centers of the two horn antennas, the metallic aperture, and the two absorbing apertures were aligned in a line. When using this setup, the horn antennas were connected to VNA by coaxial cables with SMA (SubMiniature version A) connectors. A torque wrench of 5 in/lbs preset torque was used for connection with minimized damage. Before measurement, the setup is calibrated with thru-reflect-line (TRL) standard[30, 31] to enhance signal-to-noise ratio (SNR). For 'reflect' standard, aluminum plate of same thickness with the metallic aperture was prepared. For 'line' standard (90° phase shift of the center frequency of the band), both antennas were moved 2.5 mm backward from the aperture with respect to the position of 'thru' standard. With proper calibration, transmittance and reflectance of the reference aperture with no mounted sample should be close to unity and zero, respectively, as shown in Figure 3.1 (c).

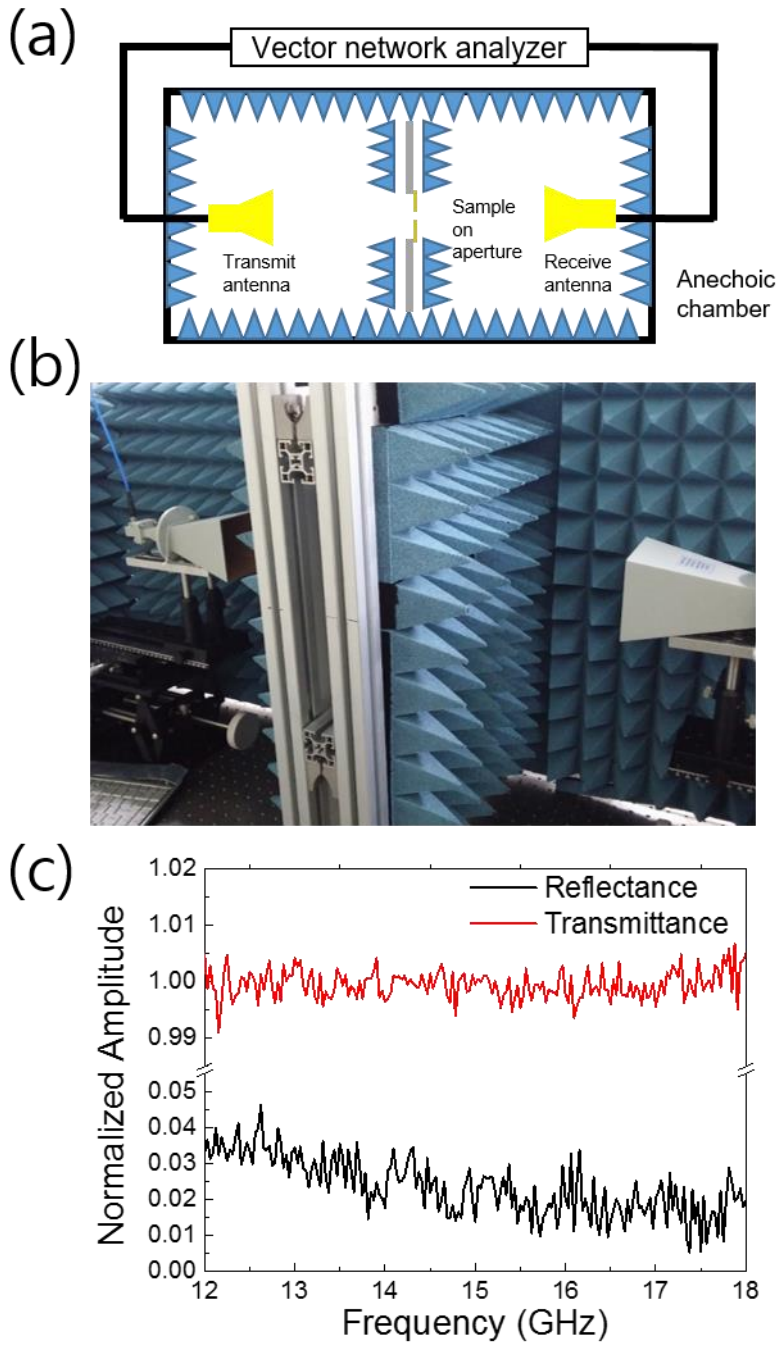

Figure 3. 1 (a) Schematic of the anechoic chamber with absorbing apertures and horn antenna pair. (b) Photograph of homemade anechoic chamber with multi octave horn antenna pair. (c) Reflectance (black) and Transmittance (red) of reference aperture right after thru-reflect-line calibration

3.2. Rectangular waveguide pair

When we approach to deeper subwavelength regime, size of the sample usually becomes smaller due to fabrication cost and transmittance tends to decrease because of small gap size and low fabrication yield. Thus a new setup with smaller beam size and enhanced SNR is demanded and rectangular waveguide can be a good alternative of horn antenna. Most of rectangular waveguide supports fundamental TE_{10} mode, most similar to free space TEM mode than any other mode, for the corresponding frequency band. The size of waveguide aperture is comparable to the areas of diffraction-limited focused waves where the diameter is $\lambda/2$. Compared to horn antenna pair, rectangular waveguide pair is more compact and less sensitive to surroundings.

Figure 3.2 (a) is the schematic cross section of rectangular waveguide pair setup. Since a slight size mismatch of waveguide and sample may cause severe noise level, size of sample is sufficiently large to cover the waveguide aperture, instead of cutting a sample to fit in the waveguide. I firstly built Ku band rectangular waveguide setup with components of calibration kit (WR62CK30, Maury Microwave) as shown in Figure 3.2 (b). This setup exhibited a moderate SNR of 30 dB due to scatterings form the holes for joint and align pin. Open-ended waveguide pair shown in Figure 3.2 (c) reached to an improved SNR of 40 dB thus I will focus on the description of the open-ended waveguide pair setup.

I built three open-ended waveguide pairs (62EWGN, 42EWGK, and 28EWGK, Chengdu AINFO inc.) for covering 12~40 GHz range.

The aperture sizes of open-ended waveguides are WR62 (15.80 mm x 7.90 mm) for Ku band (12~18 GHz), WR42 (10.67 mm x 4.32 mm) for K band (18~26.5 GHz), and WR28 (7.11 mm x 3.56 mm) for Ka band (26.5~40 GHz). The waveguide apertures were polished to be planar, smooth, and parallel to the sample surface to minimize damage to the sample and leakage of incident wave. To align each waveguide pair, tilt and rotation angles were adjusted and then centers of the waveguides were aligned in a line. After alignment, the waveguides were connected to VNA and performed TRL calibration using home-made waveguide calibration kits. The lengths of 'line' standard are 6.31 mm, 4.34 mm, and 2.92 mm for Ku, K, and Ka band, respectively. After calibration, the sample was inserted in the center of the waveguide pairs and gently clamped by the waveguide pairs to be contacted with no air gap. Transmittances were reproducible though I pressed the samples while measuring. I measured transmittance of the same sample several times while slightly rotating the samples and two angles with maximum and minimum transmittance were regarded as the p- and s-polarization cases.

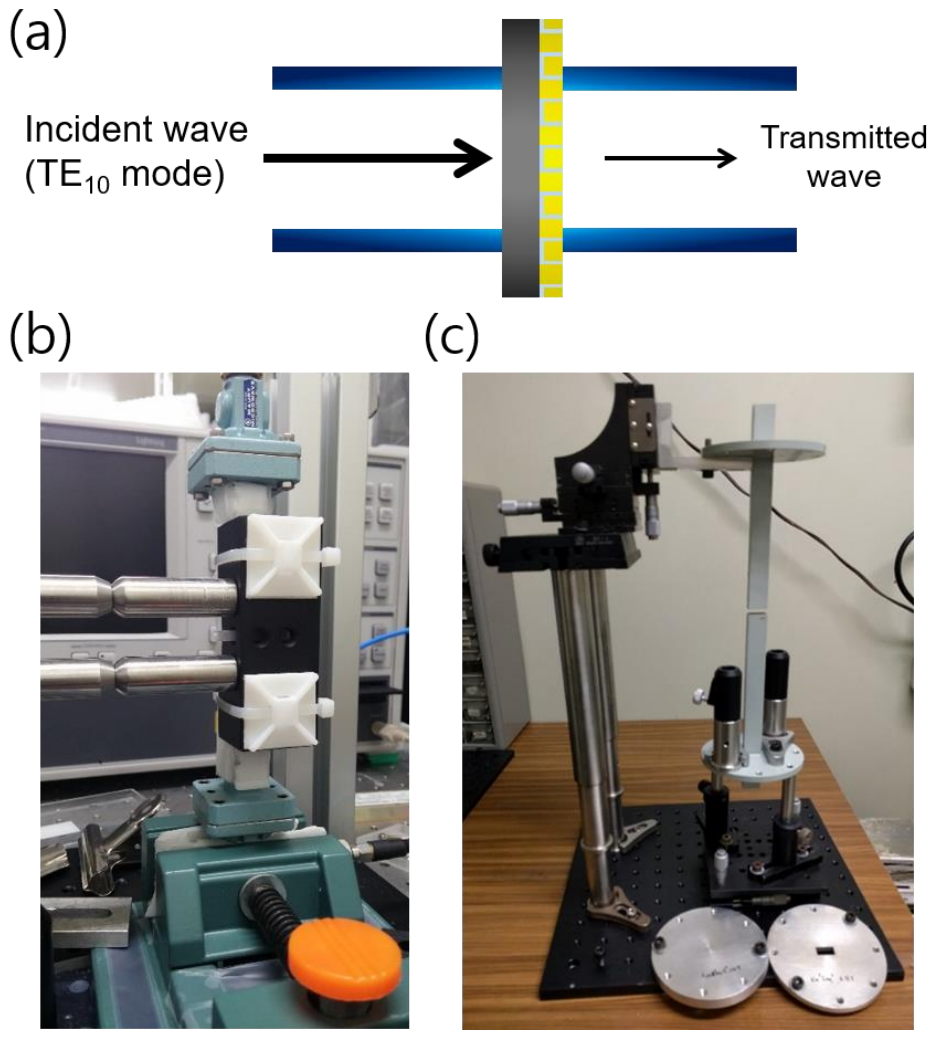

Figure 3. 2 (a) Schematic of the metallic gap sample sandwiched by open-ended waveguide pair. (b) Photograph of Ku band waveguide pair with holes for joint and align. (c) Photograph of Ku band open-ended waveguide pair and components for thru-reflect-line calibration.

3.3. Terahertz time-domain spectroscopy

The last setup I introduce is for terahertz time-domain spectroscopy (THz-TDS).[51, 52] I performed THz-TDS to measure millimeter-wave transmittance up to 1 THz. Figure 3.4 exhibits the schematic of homebuilt THz-TDS setup. A laser beam of 130 fs pulse width, 800 nm center wavelength, and 80 MHz repetition rate (Mira 900 and Verdi V5, Coherent) is divided into pump and probe beams. The pump beam impinges on an emitter, photoconductive antenna on GaAs substrate, to generate THz beam. The THz beam guided and collimated to be 2 cm diameter by parabolic mirrors (NA = 0.32) illuminates the samples mounted on an aluminum aperture. Although THz beam can be tightly focused down to 3 mm diameter, focused THz beam may not shine the whole structure since the lengths of the samples are a few millimeters and this is an improper condition for transmittance measurement. Estimated electric field strength at the sample is about 3 V/cm, not enough to observe any nonlinear phenomena.[11, 21] The transmitted beam is collected by parabolic mirrors and detected by electro-optic sampling with (110)-oriented ZnTe crystal.[53]

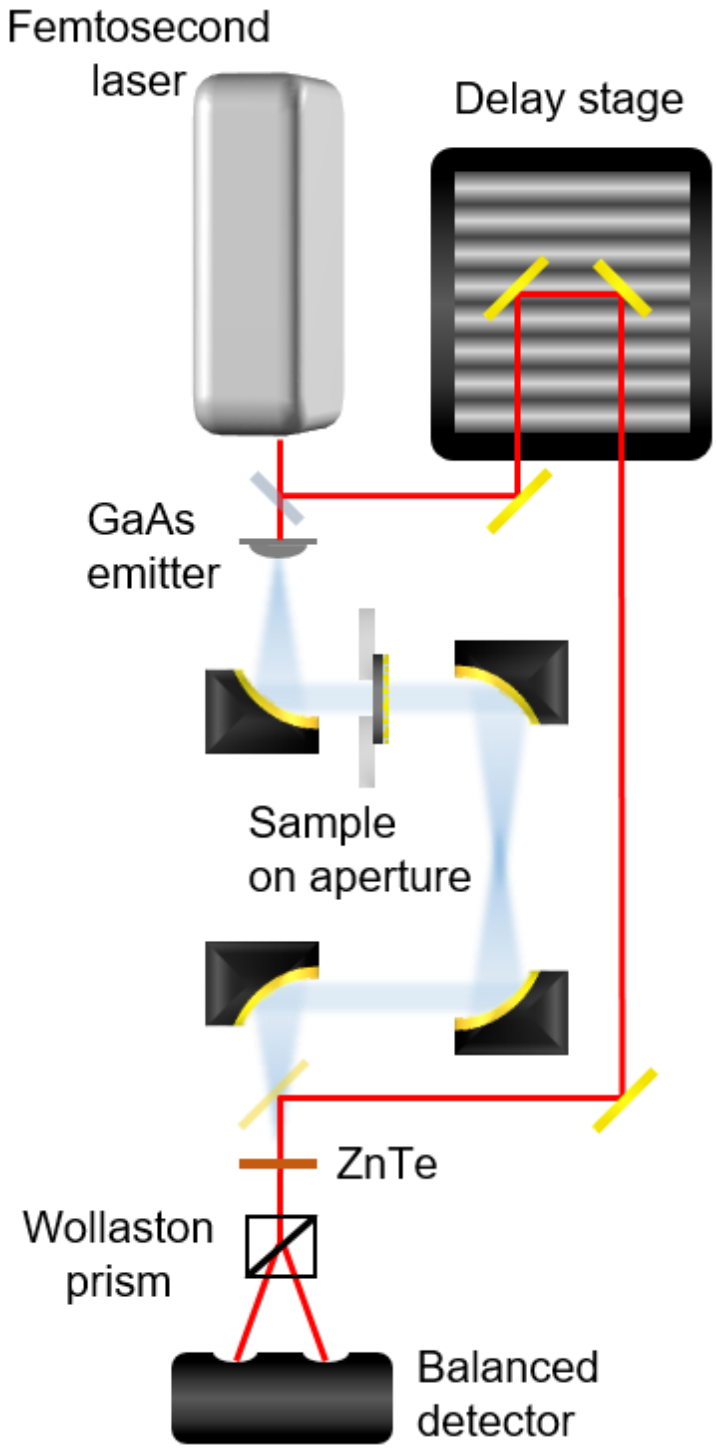

Figure 3. 3 Schematic of THz-TDS setup. The collimated THz beam illuminates the samples mounted on the metallic aperture.

Chapter 4. Microwave field enhancement by λ/400-width hand-made gaps

I prepared λ/400-width hand-made metallic gaps for microwave field enhancement, comparable to previous studies with metallic nanostructures in THz range.[32-37, 39] The samples were fabricated by perforation of aluminum foils by razor blade. The widths of the slots were about 50 μm. I also built horn antenna pair setup to measure Ku band transmittances of the samples. To verify the suitability of the hand-made gaps, I designed two microwave experiments: anomalous band formation in slot antenna arrays due to its period[35] and selective enhanced transmittance of asymmetric slot antenna pairs[37] demonstrated in THz range. Both experiments agreed well with previous studies in THz range. I will also discuss effects of fabrication errors such as slanted or tapered gaps due to perforating force.

4.1. Anomalous band formation in antenna arrays

To investigate the microwave field enhancement by λ/400-width hand-made metallic gaps, I prepared slot antenna arrays of various periods to reproduce the anomalous band formation in arrays of nano-slot antennas in THz regime.[35] Before fabrication of the sample set of varying periods, patterning area should be determined with consideration of the beam size of incident wave. Thus I made two slot antenna arrays of same geometry (10-mm-long and 50-μm-wide slot arrays of 10 mm (12 mm) period in horizontal (vertical) direction) but different sample sizes (250 mm x 300 mm and 100 mm x 100 mm). Figure 4.1 displays Ku band transmittances of those samples. The transmittance of bigger sample (250 mm x 300 mm, black line) was obtained without aperture and the smaller sample (100 mm x 100 mm) was mounted on the aperture before measurement (Details of the aperture were described in chapter 3.1.). In spite of slight differences of resonance peak and amplitude, two transmittance spectra match well considering imperfect fabrication due to human error. From this result, I patterned the samples of 10 cm x 10 cm size to decrease fabrication time and human error.

Figure 4.2 is a schematic of hand-made slot arrays with 5, 10, 15, 20, 25 mm periods. The length of each slot was set as 10 mm to be resonant in Ku band. Incident polarization was horizontal direction, perpendicular to the long axis of the slots. Since the incident wave was linearly polarized, it was assumed that interaction between slots in vertical direction was negligible.

Figure 4.3 (a) exhibits transmittances of slot antenna arrays. To

measure transmittances, the horn antenna pairs were connected to VNA (Lightning 37247D, Anritsu) and calibrated with TRL standard. With increasing the period, peak amplitude decreased and peak frequency showed red shift. When the period was changed to 25 mm, however, peak frequency suddenly moved toward higher frequency. Such non-monotonic behavior stems from the oscillatory nature of long-range coupling between slots and this is one of key points of anomalous band formation in THz nano-slot arrays. Figure 4.3 (b) shows field enhancement factors of the samples. Field enhancement can be deduced from a normalized-to-area transmittance: transmittance divided by a ratio of transparent and opaque area. When the period increased, peak amplitude of field enhancement factor was also changed in a non-monotonic way. Calculated field enhancement factor of single slot based on coupled mode theory[54] (black line in Figure 4.3 (b)) was well matched to experimental one of the slot antenna array of 10 mm period that couplings between slots were canceled out. Note that the trend and amplitude of changes in field enhancement factors of THz nano-slots and microwave hand-made slots are very similar, since the ratio of wavelength and width of slots is in same order of magnitude.

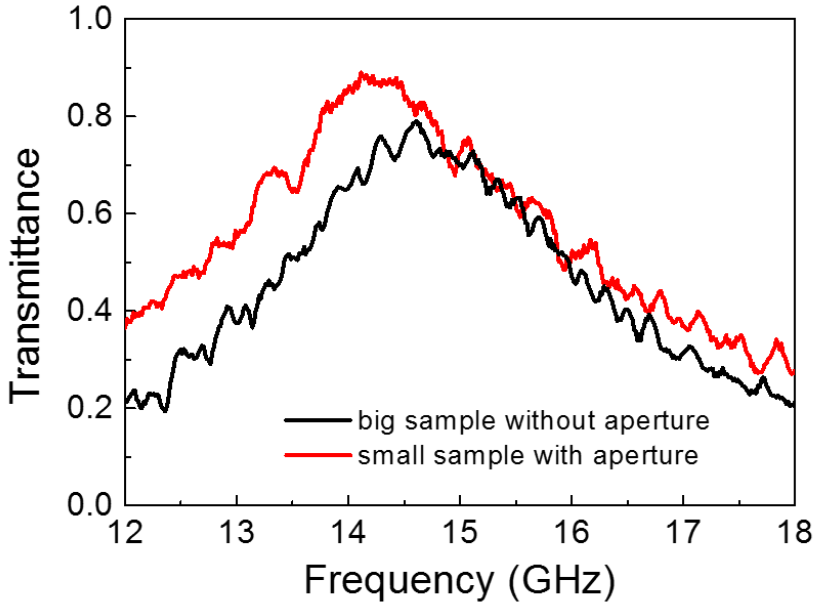

Figure 4. 1 Ku band transmittances of 10-mm-long and 50-□m-wide hand-made slot antenna arrays with different sample sizes. (Black line) Transmittance of 250 mm x 300 mm sized sample without apertures in the center of anechoic chamber. (Red line) Transmittance of 100 mm x 100 mm sized sample mounted on the metallic aperture sandwiched by absorbing apertures.

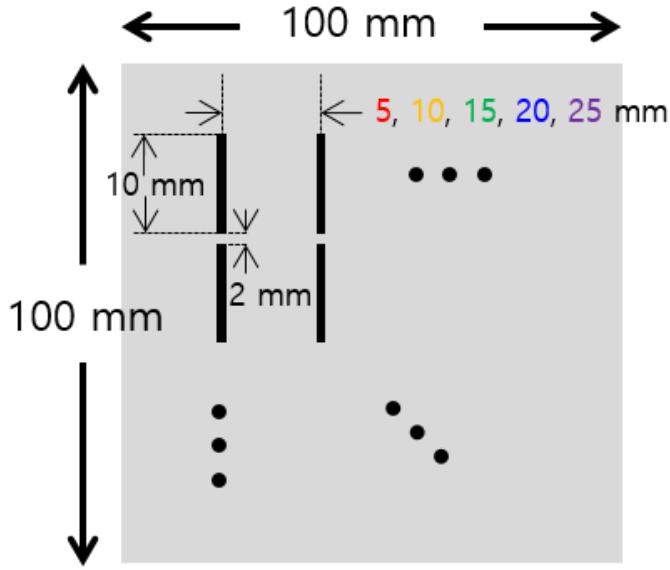

Figure 4. 2 Schematic of 50-μm-wide hand-made slot arrays with periods of 5, 10, 15, 20, 25 mm.

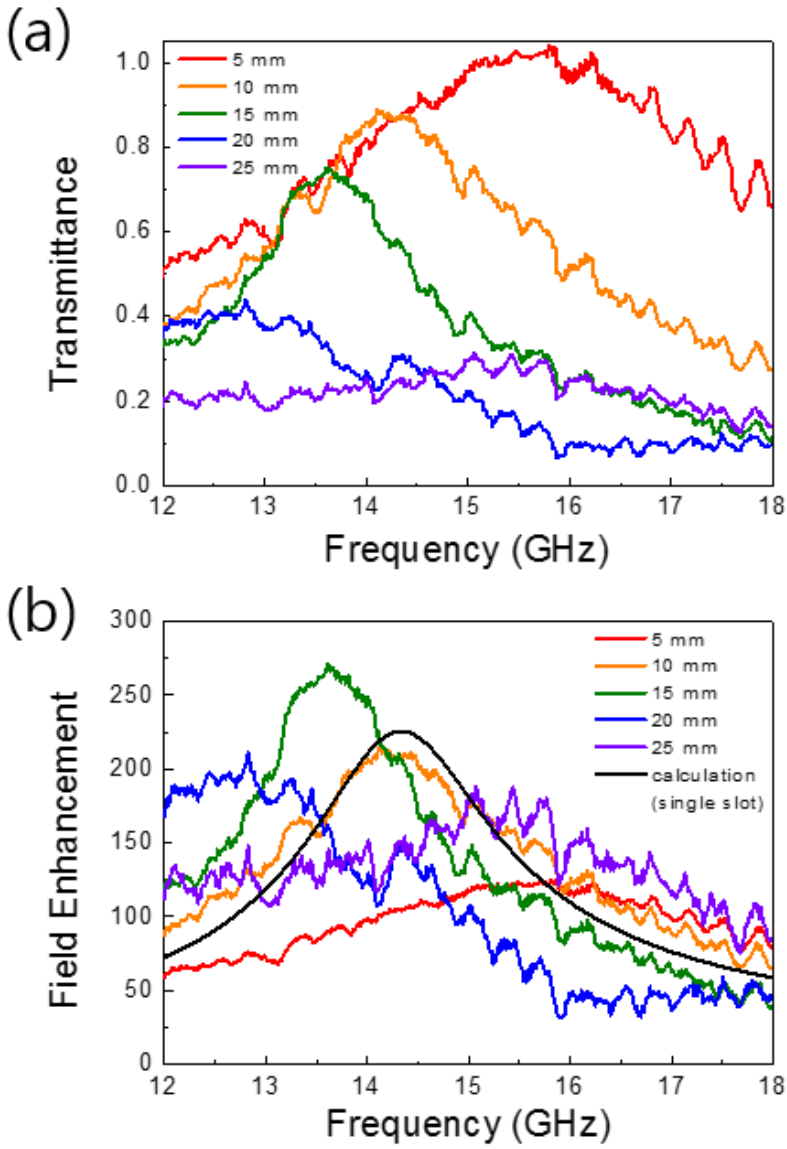

Figure 4. 3 (a) Transmittance and (b) field enhancement factor of λ/400-width slot antenna arrays with varying periods, to investigate anomalous band formation in microwave range. Calculation (black line in (b)) is based on coupled mode theory.

4.2. Selective enhanced transmittances of asymmetric antenna pairs

I also prepared asymmetric pairs of slot antennas to investigate selective enhanced transmittances which were originally demonstrated in THz range.[37] As seen in Figure 4.4, 9-mm-long and 10-mm-long slots with 1, 5, 10, 15, 20 mm separation were patterned in 100 mm x 100 mm aluminum foil. The centers of 10-mm-long and 9-mm-long slot were aligned in a row. Incident polarization was vertical to the long axes of the slots, same as chapter 4.1.

Figure 4.5 (a) presents transmittances and field enhancement factors of the samples measured by the horn antenna setup. One can find that peak amplitudes at two resonance frequencies were selectively enhanced due to changes in distances between two slots. Physical origin of this phenomenon is oscillatory behavior of coupling term, same as anomalous band formation in chapter 4.1. Calculations using coupled mode formalism (Figure 4.5 (b)) confirms the validity of experimental results.

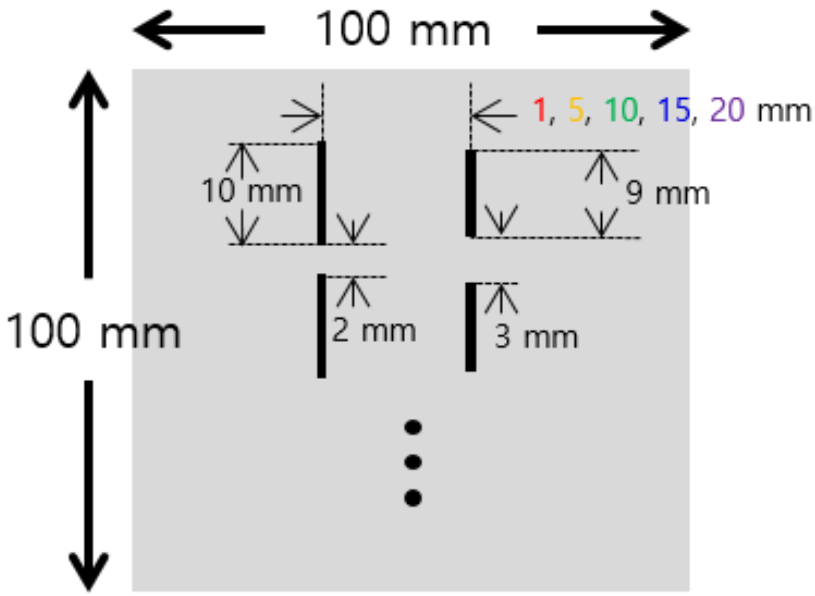

Figure 4. 5 Schematic of asymmetric pairs of 10-mm-long and 9-mm-long slots with 1, 5, 10, 15, 20 mm separation. Width of the slots is 50 μm.

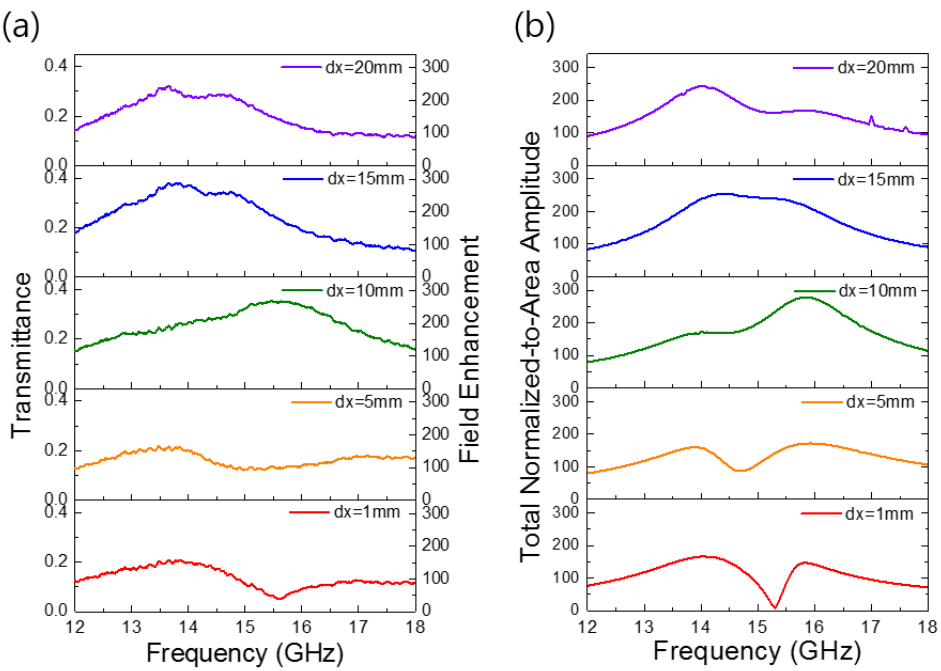

Figure 4. 4 (a) Experimental transmittances and field enhancement factors of asymmetric antenna pairs. (b) Theoretical normalized-to-area amplitude, equivalent to field enhancement factor, calculated by coupled mode formalism.

4.3. Effects of fabrication errors

Since the hand-made metallic gaps were fabricated by perforation, metal in slotted area is not removed but bent and buried below the gap. As a result, the gap structure is not a simple hole but tapered or slanted one as shown in Figure 2.1 (c). Thus the effects of such fabrication errors should be considered.

Figure 4.6 contains numerically calculated transmittances of ideal and slanted gaps using commercial finite element method program (COMSOL). Geometrical parameters e.g. length, period, thickness, etc. were set same as that of Figure 4.1. Slanted angle was assumed to be 45°. Due to slanted gaps, peak frequency was blue shifted about 1 GHz and peak amplitude was slightly decreased. When the gap is slanted or tapered, it can be considered that effective thickness and width of the gap are changed to be thicker and narrower. Those change of geometry is responsible to the peak shift and decrease of transmittance. Figure 4.7 shows E_x field profiles in the vicinity of both ideal and slanted gaps. Despite the difference of gap structure, the field profile was similar to each other.

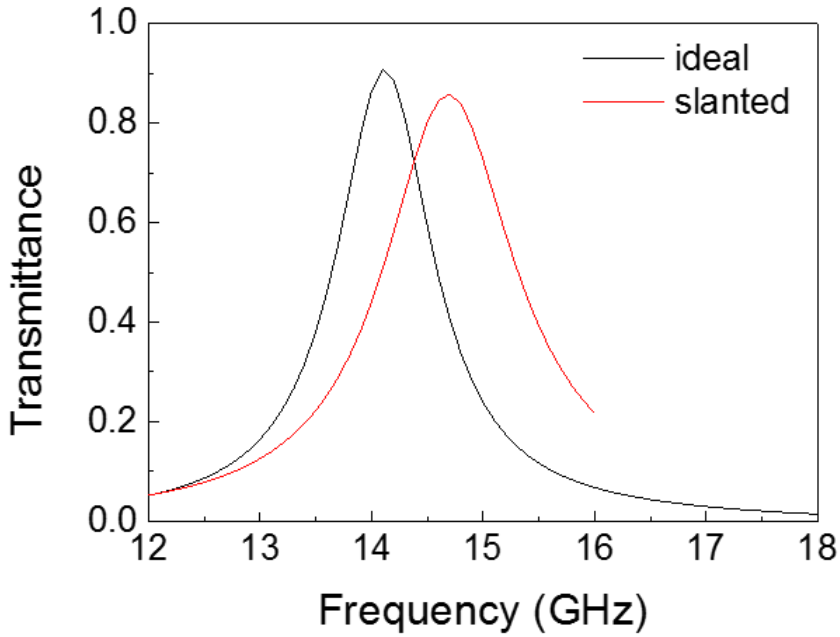

Figure 4. 7 Numerically calculated transmittances of ideal (black) and slanted (red) slots. Commercial finite element method program was used to obtain data.

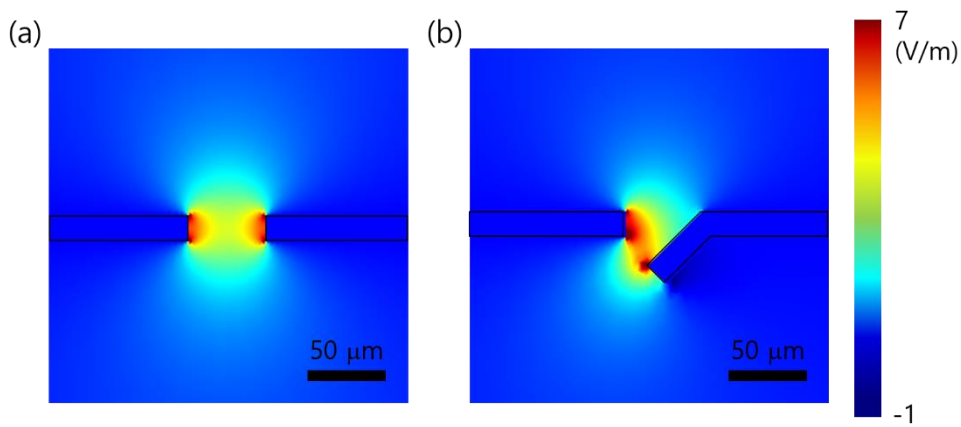

Figure 4. 6 Numerically calculated E_x field profiles in the vicinity of (a) ideal gap and (b) slanted gap. Incident field was set as 1 V/m at each resonance frequency.

4.4. Summary

In this chapter, I demonstrated that hand-made λ/400-width metallic gaps for microwave range can be good alternatives of THz nano-slots which have similar wavelength-to-width ratio. I reproduced two studies, anomalous band formation and selective enhanced transmittance in THz regime, using the hand-made slot antennas and Ku band horn antenna pairs with anechoic chamber. Although the hand-made gaps may possess fabrication errors such as slanted or tapered gap structure, these gaps can be simply regarded as thicker and narrower gaps and the differences of peak amplitude and frequency are not severe. The hand-made gaps would be a time- and cost-effective strategy for studying deep subwavelength millimeter-wave optics which uses e-beam lithography or FIB milling.

Chapter 5. Microwave field enhancement by λ/10,000,000-width nanogaps

I demonstrated microwave funneling through metallic gaps of nanometer-scale width, corresponding to λ/10,000,000. For achieving both resonant transmission and strong confinement of microwaves, two types of samples with an extreme aspect ratio, 300 nm wide, 3.5 mm long slots and sub-10 nm wide rectangular rings with a perimeter of 6.5 mm, were fabricated. Considering the gaps cover only 0.023% and 0.01% of the sample surfaces, the magnitudes of electric fields inside the gaps increase up to 1,400-fold and 5,000-fold, for the nano-slots and the nanogap rings, respectively.[33, 54] The polarization extinction ratio up to 20 dB indicates that the microwave transmission originates from capacitive coupling of the induced charges at the sidewalls of a metallic gap. The essential physics is as follows: incident magnetic-field induced current density of $2H_{inc}/h$ (h=film thickness) charges the gap, which translates into huge electric field enhancement of the order of $\lambda/\pi nh$ where n is the index of refraction.[55, 56] I also measure terahertz transmittance and observe a convergence to the microwave range. This work represents the highest field enhancement recorded for the microwave regime, made possible by wafer-scale-length nanogaps matching the wavelengths, with future applications in centimeter wave nonlinearities and enhanced detection sensitivities.

5.1. Field enhancement by λ/2,000-width gaps

In the previous chapter, I described about microwave field enhancement by λ/400-width hand-made gaps measured by horn antenna pair. To study microwave field enhancement in deeper subwavelength regime, metallic gaps made by nanofabrication techniques are mandatory. New experimental setup is also essential to maintain reasonable SNR for smaller samples and narrower gaps.

In this section, I will state about microwave field enhancement by λ/2,000-width gaps in prior to λ/10,000,000-width gaps, the main goal of this chapter. Figure 5.1 (a) represents schematics of the positive and negative antennas fabricated by photolithography. The samples are same as Figure 2.2. Transmitted amplitudes and field enhancement factors in Figure 5.1 (b) and (c) were measured by rectangular waveguide pair introduced in Figure 3.2 (b). One can find that negative (positive) antenna resonates at about 15 GHz with p- (s-) polarized wave in Figure 5.1 (b). With improper polarization, negative antenna shows nearly zero transmitted amplitude (black dashed) and positive antenna (red solid) acts like bare substrate (blue solid). Experimental field enhancement factor of negative antenna agrees well with calculation by coupled mode theory, as shown in Figure 5.1 (c). Above results confirms validity of waveguide pair setup for measurement of deeper subwavelength antennas.

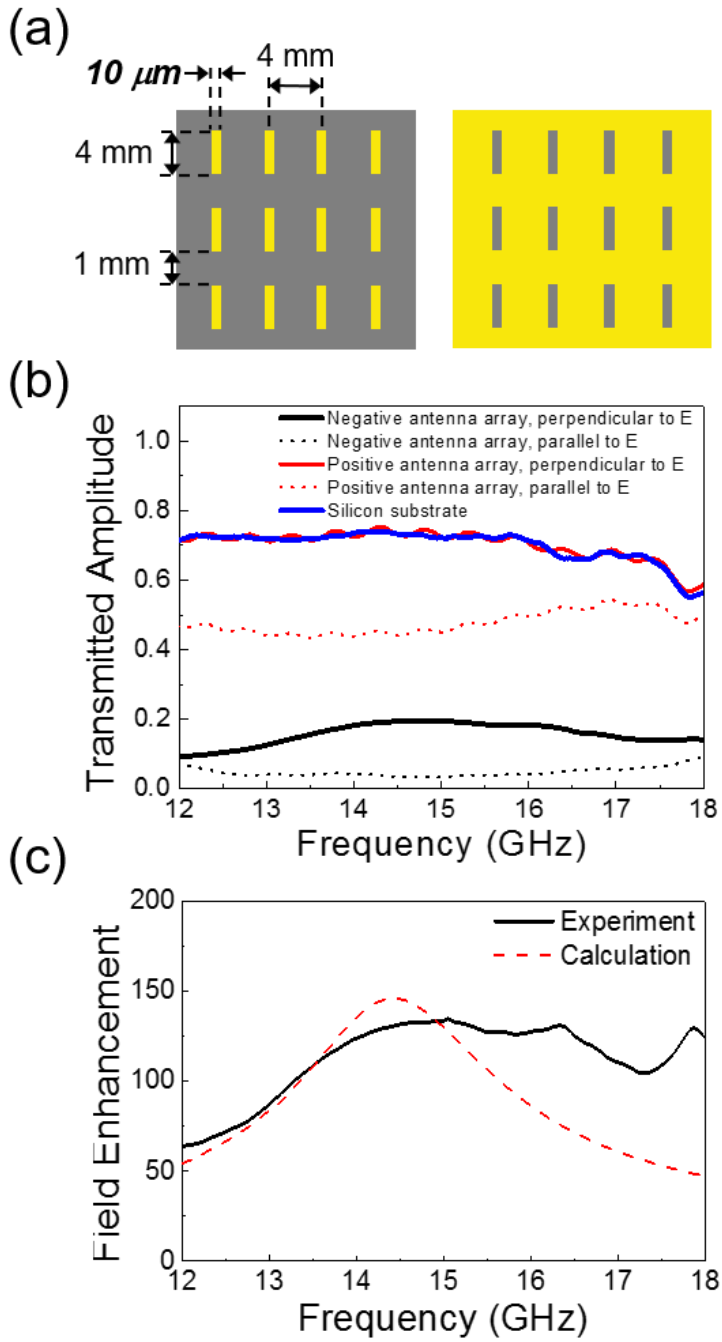

Figure 5. 1 (a) Schematics of λ/2,000-width positive (left) and negative (right) antenna array. 3 nm Cr and 97 nm Au layer were deposited on undoped Si substrate for both samples. (b) Transmitted amplitudes of antennas and substrate with different polarizations. (c) Field enhancement factor of negative antennas obtained by experiment and calculation by coupled mode theory.

5.2. Details on the nanogap sample

To investigate further subwavelength regime, the nano-slot array was milled by FIB and the nanogap rings array was patterned by the modified atomic layer lithography.[29] The gap widths are 300 nm and 5 nm for the nano-slots and the nanogap rings, respectively. Detailed parameters of the samples are given in Figure 5.1. After fabrication, I took top-view and cross sectional images of the samples to confirm the successful metallic gap formation. Figure 2.3 is the images of the nano-slots measured in this chapter. The images of the nanogap rings are shown in Figure 5.2. I used optical reflection microscope and field enhanced scanning electron microscope (FE-SEM, TESCAN) were used to obtain top-view and cross sectional images of the samples. To gain optical dark field image, the nanogap rings were slanted so that reflected beams would not be collected by objective lens (5x, numerical aperture (NA) = 0.15) and only scattered lights from the nanogaps can be imaged. Asymmetric lines of the dark field image are due to the slanted angle of the sample. To acquire cross sectional image, platinum was deposited on the gap and cut by FIB combined with FE-SEM. Platinum on the top prevents damages to the nanogaps while proceeding gallium ion beam milling. As shown in Figure 5.2 (a) and (b), the nanogaps of 50 μm x 3,200 μm rectangular ring array were successfully fabricated over large area. The SEM cross section of the nanogap ring (Figure 5.2 (c)) clearly shows the dielectric gap of sub-10-nm width, corresponding to λ/10,000,000.

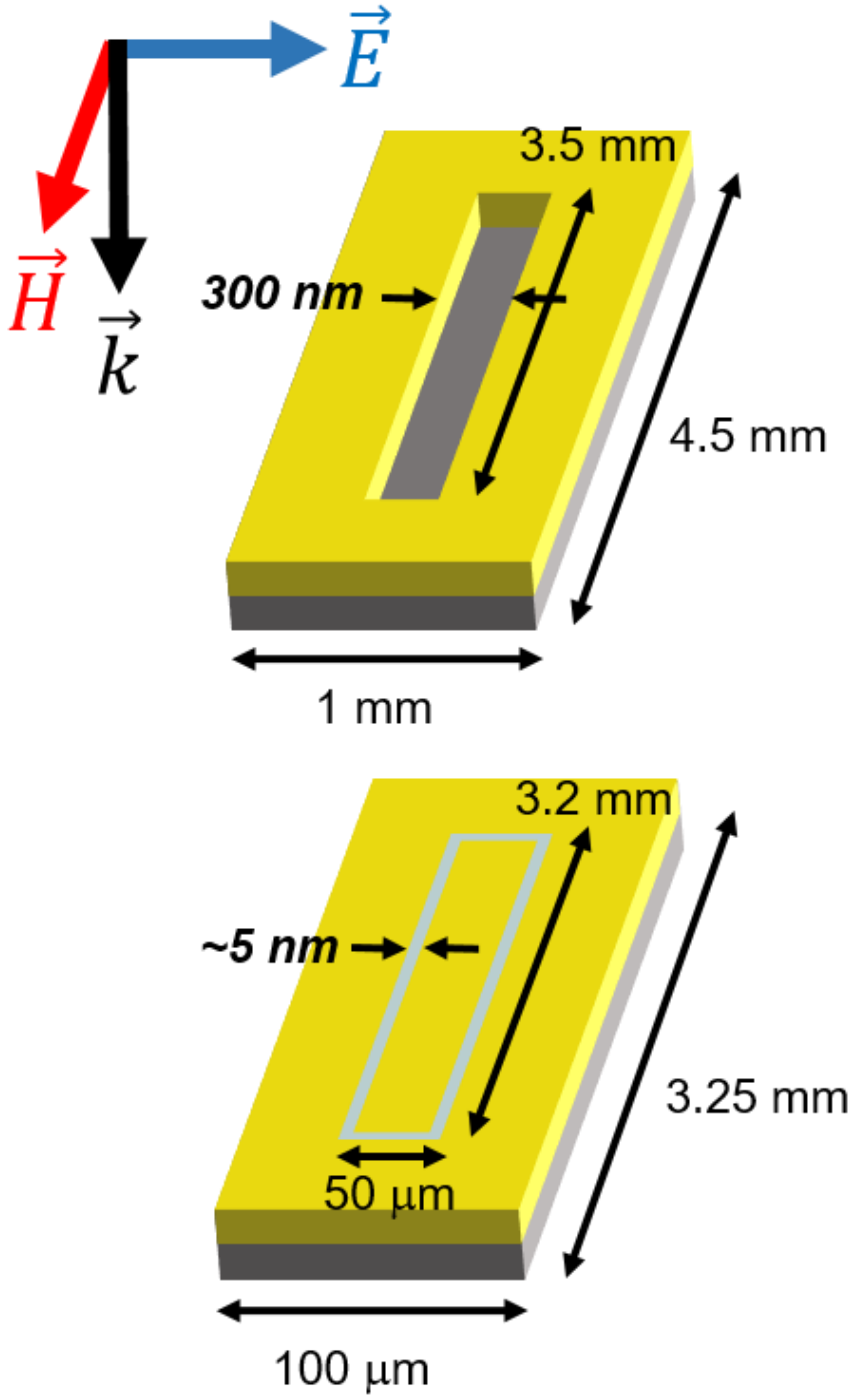

Figure 5. 2 Schematic of (top) the nanoslot made by FIB and (bottom) the nanogap ring fabricated by the modified atomic layer lithography under a p-polarized incident wave.

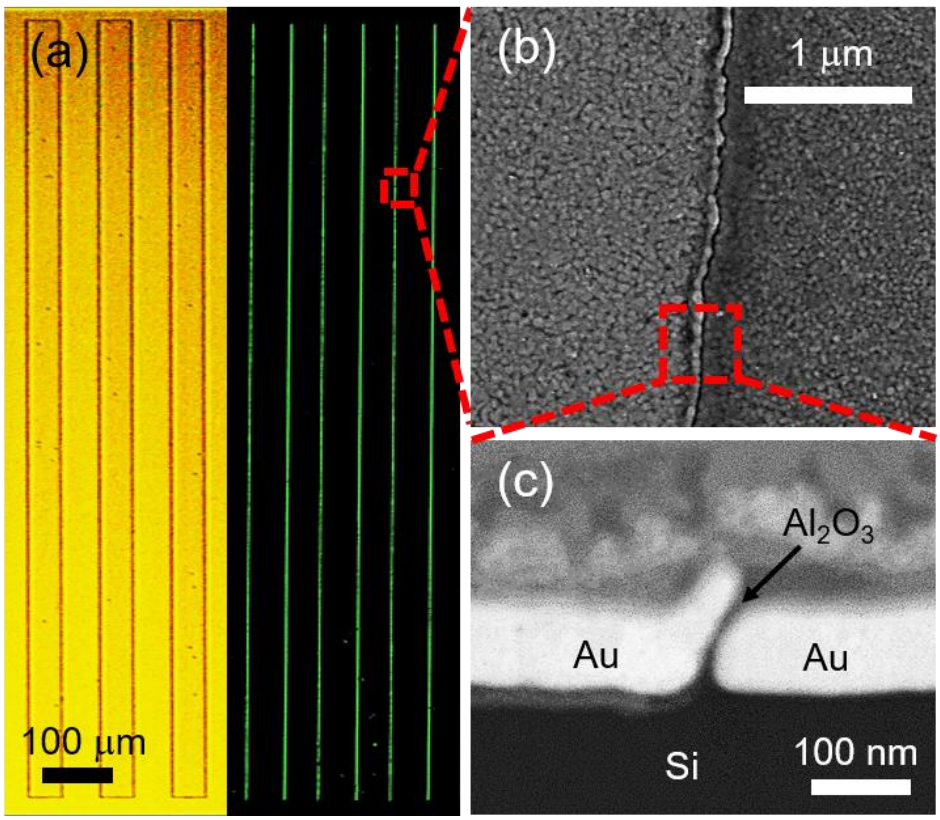

Figure 5. 3 Images of the nanogaps fabricated by the modified atomic layer lithography. (a) Top-view optical micrographs of 50 μm x 3,200 μm rectangular ring array with sub-10-nm-wide gap. The images are reduced in the vertical direction to show the whole ring structure. (Left) reflection image (right) dark field image under p-polarized illumination. (b) Top-view SEM image. (c) Cross sectional SEM image.

5.3. Microwave transmission measurements

I measured microwave transmittances of the nanogap samples to observe funneling behavior. The samples were sandwiched by open-ended waveguide pairs connected with VNA (Vectorstar MS4644A, Anritsu). Three open-ended waveguide pairs are used to cover 12~40 GHz range with fundamental TE_{10} mode. Power from VNA was about 10 mW, far below a breakdown limit of the dielectric spacer and nonlinear regime.[21] Each open-ended waveguide pair is calibrated by TRL standard before measurement. Figure 5.3 is the microwave transmittances of both nanogap samples and unpatterned gold film under p- and s-polarized incident waves. Transmitted microwave amplitudes from the samples are normalized with those of bare substrates. The microwave transmittances under p-polarization show broad but resonant features and are clearly distinguished with that of s-polarization and unpatterned gold film. The polarization extinction ratio reaches up to 20 dB at the peak transmittance of the nanogap rings. These strong transmission of p-polarized wave indicates the capacitive coupling of induced charges and electric field enhancement at the gaps, as reported in previous studies at THz range.[33] Although the skin depth of gold at microwave regime (about 700 nm) is much larger than the thickness of the sample (97 nm), most of the incident wave is reflected at the metal-air interface due to the high permittivity of gold. Therefore, direct transmission through metal layer is very low ~0.5% and spectrally flat, resulting in the near-zero transmittance of unpatterned gold film shown in Figure 5.3. Clearly, funneling at the nanogaps dominates the transmission.

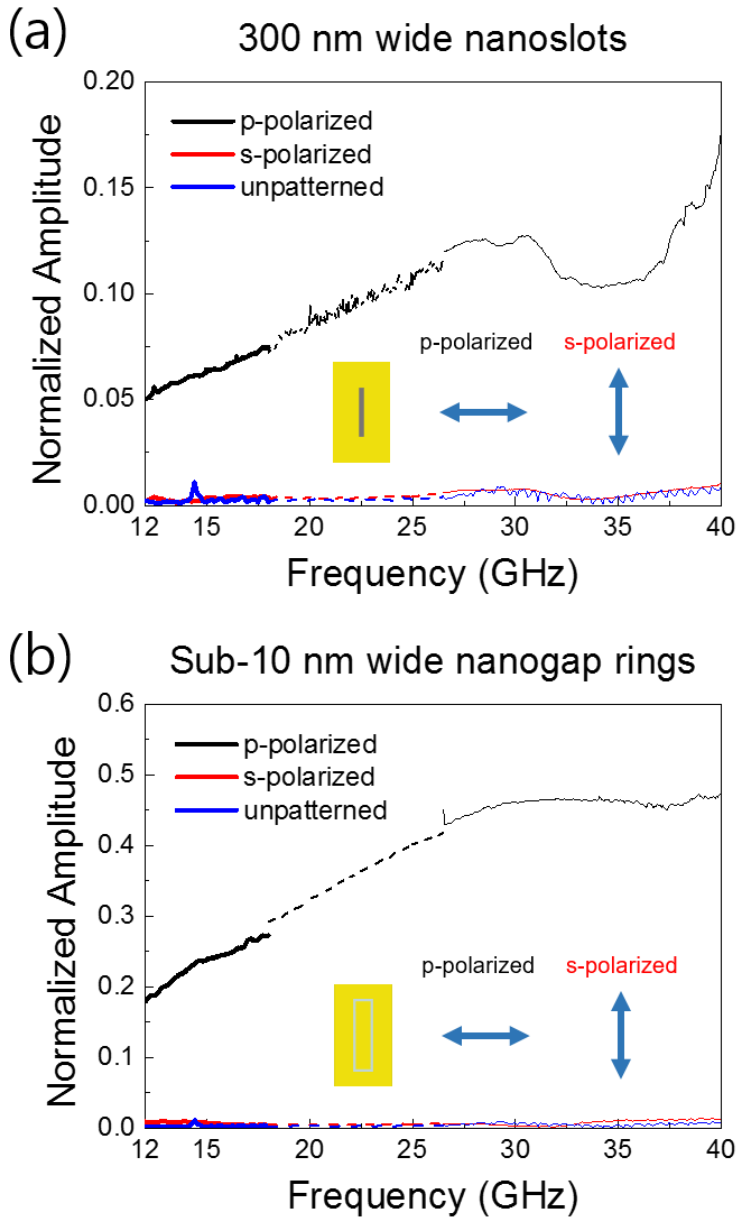

Figure 5. 4 Microwave transmittances through the nanogaps. (a) Microwave transmittance of the 300-nm-wide nano-slot antenna array. (b) Microwave transmittance of the sub-10-nm-wide nanogap rings array. Transmitted amplitudes of the samples with p- and s-polarized incident wave and unpatterned gold film of the same thickness are normalized with those of bare substrate. Transmittances are measured in the three frequency ranges: Ku (12~18 GHz, thick solid), K (18~26.5 GHz, dashed), and Ka (26.5~40 GHz, thin solid) band.

5.4. Comparison with terahertz time-domain spectroscopy

I performed THz-TDS on the samples for comparison with microwave transmittance. To avoid evanescent decay from small aperture below a cut-off frequency and any effects from frequency dependent spot sizes, the samples are mounted on large aluminum apertures (1 cm x 1 cm for the nano-slots, 1.6 cm x 1.6 cm for the nanogap rings) and illuminated by a collimated THz beam. The scanning time is set at 200 ps for capturing low frequency components. The frequency resolution is 5 GHz, the reciprocal of the scanning time. Figure 5.4 exhibits time-traces of transmitted THz wave through a bare aluminum aperture, substrate, and the nanogaps under p- and s-polarizations. Multiple peaks with 11.45 ps intervals from the substrate originate from the Fabry-Pérot (FP) resonance related to the thickness of 500 μm and the refractive index of 3.435, nearly a constant value in the frequency range of interest.[57, 58] The sign of second peak from the nanogaps is inverted due to π-phase shift at the metal-substrate interface.

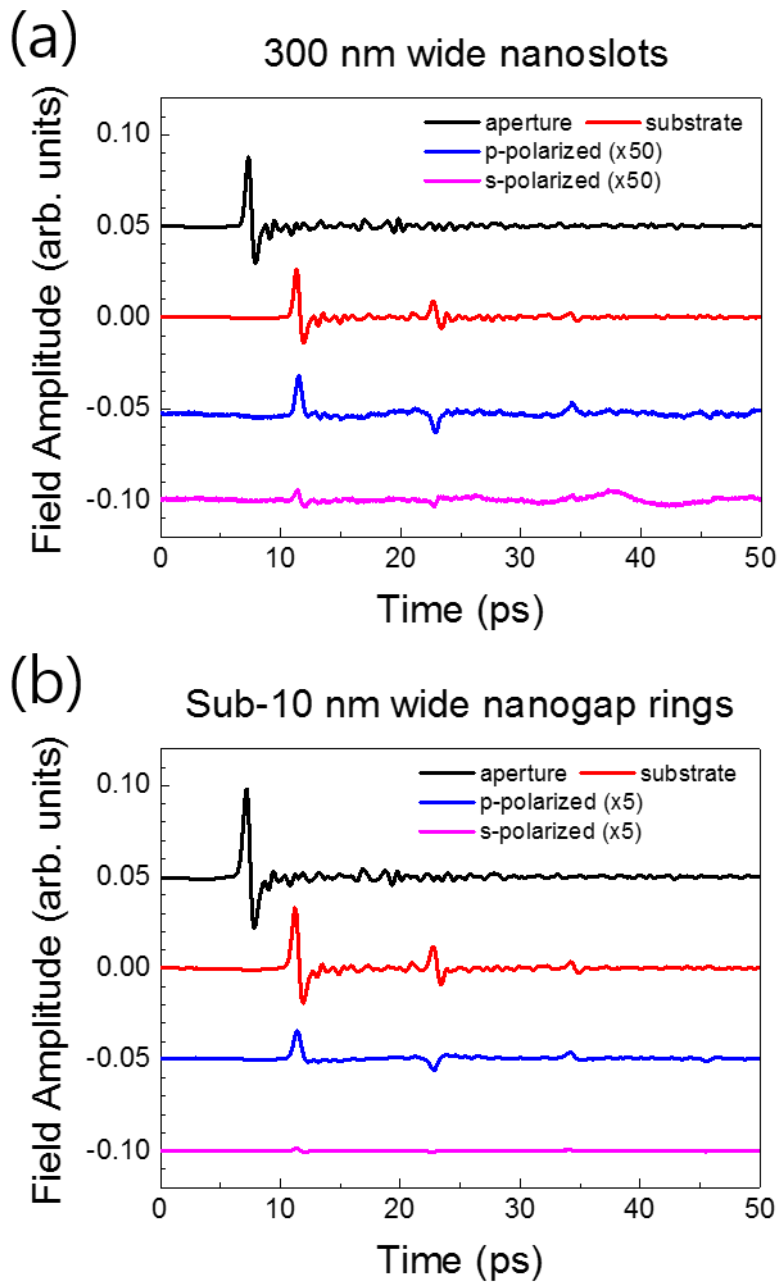

Figure 5. 5 Time traces of transmitted THz waves through (a) the 300-nm-wide nano-slots and (b) the sub-10-nm-wide nanogap rings. Scanning time range was 200 ps with 0.05 ps resolution.

Figure 5.5 contains the log-scale plots of microwave and THz transmittance of the nano-slots and the nanogap rings, respectively. I subtracted the transmitted THz amplitude through unpatterned gold film in time-domain, calculate transmitted amplitude spectra by Fourier transform, and finally obtain transmittance by normalization with bare substrate. Microwave and THz transmittance measurements were fully consistent within their respective overlap regions, enabling a unified picture of the whole range. Slight mismatch of transmittance in Figure 5.5 (b) is mainly due to a low SNR of THz-TDS at the lower limit of frequency and does not break the consistency of the experiments. I deduced electric field enhancement factor of the nanogaps from dividing normalized transmitted amplitude by the coverage ratio of the gap area in the sample surface.[32, 33] The peak values of field enhancement reached 1,400 for the 300-nm-wide nano-slots and 5,000 for the nanogap rings with 5 nm gap width (estimated by Figure 5.2 (c)). These giant values are still below the theoretical limit of slit structure[59] and the experimental record of the nanogap rings in THz regime,[8] due to the overpopulation of patterns in the samples.[35] It is expected that further enhancement of microwave field inside the nanogaps would be achieved with optimized geometries.

The fundamental resonance of the ring structure occurs when the perimeter of the ring matches with wavelength, after having taken care of the effective index of refraction of the air-substrate composite.[38] On the other hand, the fundamental resonance of the slot structure takes place when the length of the slot matches a half of wavelength. In this work, the length of the nano-slot is 3.5 mm and the perimeter of the nanogap ring is 6.5 mm. Owing to these length scales and substrate effect, theoretically expected resonance frequencies of both samples fall

into the centimeter wave range. Calculations by modal expansion method[54] with consideration of gap plasmon[60] (blue lines in Figure 5.5) predict the fundamental resonances of both samples at 19 GHz, departing significantly from the experimental peaks occurring at wavelength of about 1 cm (30-40 GHz) for both samples. The effects of FP resonances on the measured transmittances can be partially removed by straightforward calculations from air-substrate-air problems[61] (red lines in Figure 5.5), with care of the π-phase shift from the metal-substrate interface, and the results show fundamental resonance peaks agreeing better with calculations.

It is noted that experiments and calculations agreed well at terahertz frequency ranges, while the experimental enhancement values are significantly smaller at microwave frequencies. The differences of experimental and theoretical transmittance magnitudes may come from non-zero conductivity of the substrate, density of patterns, fabrication errors, etc. For the nano-slots case, the fabrication process was straightforward and thus the conductivity of the substrate and the sparsity of the slots would be dominant. On the other hand, the transmittance of the nanogap rings can be significantly affected by imperfections of the samples such as asymmetric periodicity,[62] tapered gap opening,[63] defects of dielectric spacer, and debris of chemically etched metal. In particular, the defects of spacer and the metallic debris can be treated as small metallic bridges in or on the gaps. These metallic bridges provide an interesting perspective on the particle sensing with microwave. At the high frequency regime, the nano-slots and the nanogap rings would behave as effectively infinite slit structures due to their length and perimeter of over 3 mm.[33] The metallic bridges would change the high frequency transmittances of the slits from non-resonant

to high-order resonant responses and the difference of these two responses is small in terms of the peak magnitude.[64] On the other hand, the fundamental resonances of the nano-slots and the nanogap rings would be dominant at the low frequency regime and these are intimately affected by the small bridges of individual slots or rings.[36, 65] Therefore, surprisingly, microwave may be more sensitive than THz and visible lights to the overall defects of the whole ring structure, making it a useful tool to investigate wafer-scale uniformity.

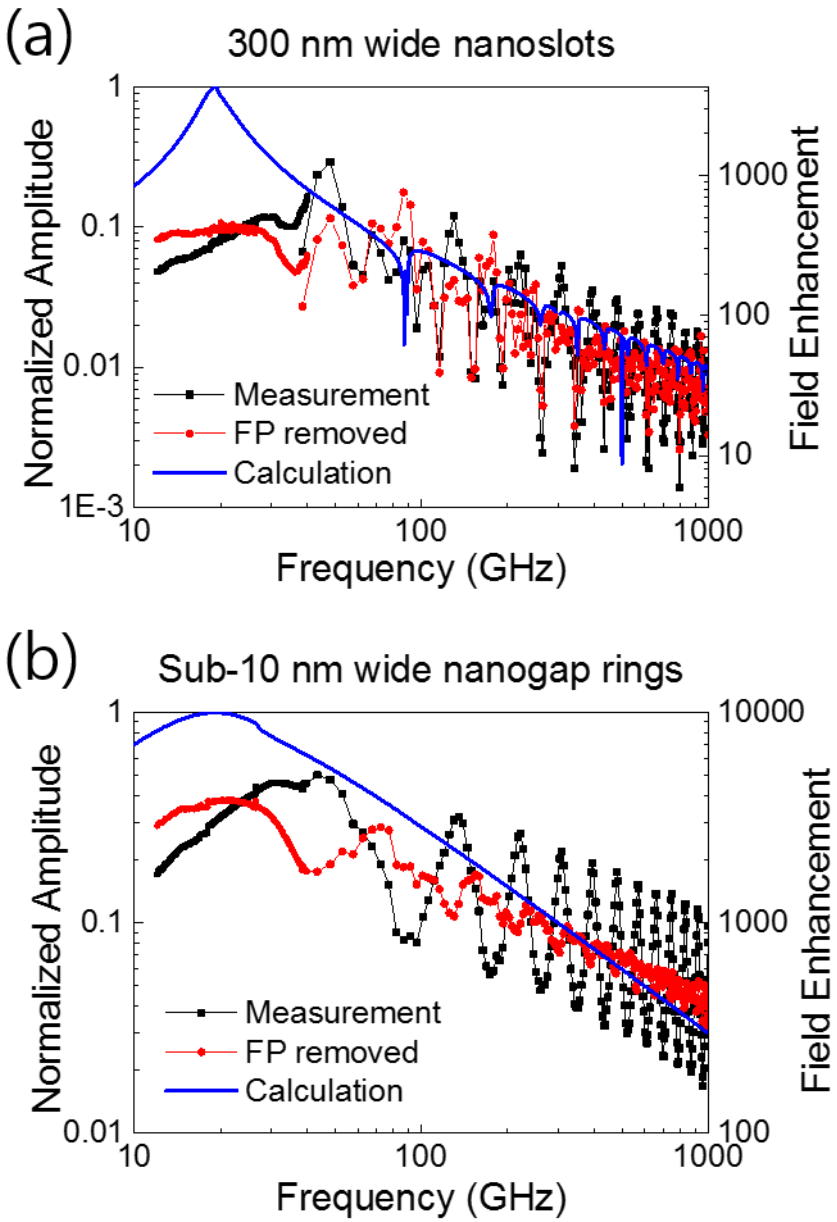

Figure 5. 6 Microwave and THz transmittances through the (a) the 300-nm-wide nano-slots and (b) the sub-10-nm-wide nanogap rings. Frequency resolution of THz-TDS was 5 GHz, the reciprocal of 200 ps scanning time range.

5.5. Summary

In conclusion, we demonstrate microwave funneling through 300-nm-wide nano-slots and sub-10-nm-wide nanogap rings. The nano-slots are milled by FIB and the nanogap rings are fabricated by atomic layer lithography. Microwave and THz transmittances reach up to 30% for the nano-slots and 50% for the nanogap-rings. By considering the 0.01% coverage ratio of the gap area in the sample surface, estimated field enhancement factor reach values of 1,400 and 5,000. The fundamental resonances are at the wavelengths of about 1 cm, due to the combination of the nanogap geometries and FP resonances from substrates. This work is the first demonstration of resonant microwave transmission through nanometer-sized structures, squeezing electromagnetic wave in the $\lambda/10{,}000{,}000$ scale.

Chapter 6. Conclusions

In conclusion, I investigated microwave field enhancement by deep subwavelength metallic gaps down to 5 nanometers. In λ/400-width regime, I successfully reproduced two previous studies using nano-slots and terahertz time-domain spectroscopy, anomalous band formation and selective enhanced resonances, with hand-made gaps and horn antenna pair operating in Ku band. The hand-made gap would be a time- and cost-efficient tool for studying deep subwavelength optics. In much deeper subwavelength regime, I prepared nanogap rings by atomic layer lithography and observed extreme funneling through λ/10,000,000-wide gaps and strong field enhancement up to 5,000-fold. This work is the first experimental demonstration of microwave funneling through nano-resonators.

I would like to introduce a microwave switching device as a potential application of microwave field enhancement via subwavelength structures. The switching device is based on an insulator-to-metal transition material and deep subwavelength slot antennas. By the subwavelength metallic gaps, incident field is strongly confined nearby the gaps so that the wave can be effectively controlled with very thin layer of functional materials. Vanadium dioxide (VO_2) was selected to implement microwave switching device due to its insulator-to-metal transition characteristic. The concept was already demonstrated in several terahertz studies[16, 66-68] and in this work, a microwave switching device was designed and measured for Ku band range.

The aforementioned studies would provide a way of reaching to much deeper subwavelength optics, enhancing functionalities of microwave and millimeter-wave optical devices, and controlling molecules and liquids non-invasively.

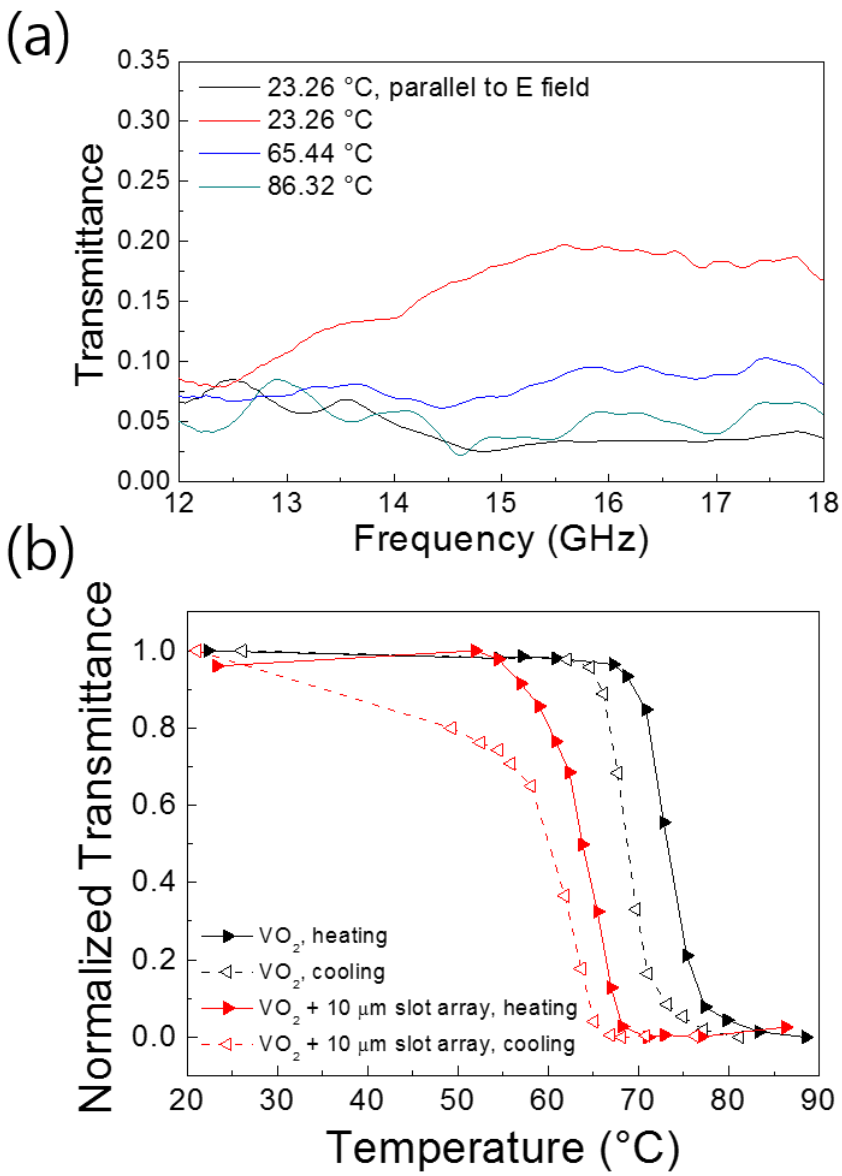

Figure 6. 1 (a) Transmittances of 4-mm-long and 10-mm-wide slot antenna array patterned on 150-nm-thick VO_2 film. (b) Hysteresis curves of transmittances of bare VO_2 film and antennas on VO_2 film. Each transmittance is normalized with its maximum value.

Bibliography

1. Ebbesen, T. W.; Lezec, H. J.; Ghaemi, H. F.; Thio, T.; Wolff, P. A. Extraordinary optical transmission through sub-wavelength hole arrays. Nature 1998, **391**, 667-669.

2. Lee, J. W.; Seo, M. A.; Kim, D. S.; Jeoung, S. C.; Lienau, C.; Kang, J. H.; Park, Q. H. Fabry–Perot effects in THz time-domain spectroscopy of plasmonic band-gap structures. Applied Physics Letters 2006, **88**, 071114.

3. Miyazaki, H. T.; Kurokawa, Y. Squeezing Visible Light Waves into a 3-nm-Thick and 55-nm-Long Plasmon Cavity. Physical Review Letters 2006, **96**, 097401.

4. Seo, M. A.; Adam, A. J. L.; Kang, J. H.; Lee, J. W.; Ahn, K. J.; Park, Q. H.; Planken, P. C. M.; Kim, D. S. Near field imaging of terahertz focusing onto rectangular apertures. Opt. Express 2008, **16**, 20484-20489.

5. Garcia-Vidal, F. J.; Martin-Moreno, L.; Ebbesen, T. W.; Kuipers, L. Light passing through subwavelength apertures. Reviews of Modern Physics 2010, **82**, 729-787.

6. Nien, L.-W.; Lin, S.-C.; Chao, B.-K.; Chen, M.-J.; Li, J.-H.; Hsueh, C.-H. Giant Electric Field Enhancement and Localized Surface Plasmon Resonance by Optimizing Contour Bowtie Nanoantennas. The

Journal of Physical Chemistry C 2013, **117**, 25004-25011.

7. Ciraci, C.; Hill, R. T.; Mock, J. J.; Urzhumov, Y.; Fernandez-Dominguez, A. I.; Maier, S. A.; Pendry, J. B.; Chilkoti, A.; Smith, D. R. Probing the ultimate limits of plasmonic enhancement. Science 2012, **337**, 1072-4.

8. Chen, X.; Park, H. R.; Pelton, M.; Piao, X.; Lindquist, N. C.; Im, H.; Kim, Y. J.; Ahn, J. S.; Ahn, K. J.; Park, N.; Kim, D. S.; Oh, S. H. Atomic layer lithography of wafer-scale nanogap arrays for extreme confinement of electromagnetic waves. Nat Commun 2013, **4**, 2361.

9. Chen, X.; Park, H. R.; Lindquist, N. C.; Shaver, J.; Pelton, M.; Oh, S. H. Squeezing millimeter waves through a single, nanometer-wide, centimeter-long slit. Sci Rep 2014, **4**, 6722.

10. Ward, D. R.; Huser, F.; Pauly, F.; Cuevas, J. C.; Natelson, D. Optical rectification and field enhancement in a plasmonic nanogap. Nat Nanotechnol 2010, **5**, 732-6.

11. Bahk, Y. M.; Kang, B. J.; Kim, Y. S.; Kim, J. Y.; Kim, W. T.; Kim, T. Y.; Kang, T.; Rhie, J.; Han, S.; Park, C. H.; Rotermund, F.; Kim, D. S. Electromagnetic Saturation of Angstrom-Sized Quantum Barriers at Terahertz Frequencies. Phys Rev Lett 2015, **115**, 125501.

12. Siegfried, T.; Wang, L.; Ekinci, Y.; Martin, O. J. F.; Sigg, H. Metal double layers with sub-10 nm channels. ACS Nano 2014, **8**, 3700-3706.

13. Zhang, Q.; Large, N.; Nordlander, P.; Wang, H. Porous Au Nanoparticles with Tunable Plasmon Resonances and Intense Field Enhancements for Single-Particle SERS. J Phys Chem Lett 2014, **5**, 370-4.

14. Park, H. R.; Ahn, K. J.; Han, S.; Bahk, Y. M.; Park, N.; Kim, D. S. Colossal absorption of molecules inside single terahertz nanoantennas. Nano Lett 2013, **13**, 1782-6.

15. Liu, M.; Hwang, H. Y.; Tao, H.; Strikwerda, A. C.; Fan, K.; Keiser, G. R.; Sternbach, A. J.; West, K. G.; Kittiwatanakul, S.; Lu, J.; Wolf, S. A.; Omenetto, F. G.; Zhang, X.; Nelson, K. A.; Averitt, R. D. Terahertz-field-induced insulator-to-metal transition in vanadium dioxide metamaterial. Nature 2012, **487**, 345-348.

16. Jeong, Y. G.; Han, S.; Rhie, J.; Kyoung, J. S.; Choi, J. W.; Park, N.; Hong, S.; Kim, B. J.; Kim, H. T.; Kim, D. S. A Vanadium Dioxide Metamaterial Disengaged from Insulator-to-Metal Transition. Nano Lett 2015, **15**, 6318-23.

17. Lassiter, J. B.; Chen, X.; Liu, X.; Ciracì, C.; Hoang, T. B.; Larouche, S.; Oh, S.-H.; Mikkelsen, M. H.; Smith, D. R. Third-Harmonic Generation Enhancement by Film-Coupled Plasmonic Stripe Resonators. ACS Photonics 2014, **1**, 1212-1217.

18. Jensen, R. A.; Huang, I. C.; Chen, O.; Choy, J. T.; Bischof, T. S.; Lončar, M.; Bawendi, M. G. Optical Trapping and Two-Photon

Excitation of Colloidal Quantum Dots Using Bowtie Apertures. ACS Photonics 2016, **3**, 423-427.

19. Mortensen, N. A.; Raza, S.; Wubs, M.; Sondergaard, T.; Bozhevolnyi, S. I. A generalized non-local optical response theory for plasmonic nanostructures. Nat Commun 2014, **5**, 3809.

20. Wu, L.; Duan, H.; Bai, P.; Bosman, M.; Yang, J. K. W.; Li, E. Fowler–Nordheim Tunneling Induced Charge Transfer Plasmons between Nearly Touching Nanoparticles. ACS Nano 2013, **7**, 707-716.

21. Kim, J. Y.; Kang, B. J.; Park, J.; Bahk, Y. M.; Kim, W. T.; Rhie, J.; Jeon, H.; Rotermund, F.; Kim, D. S. Terahertz Quantum Plasmonics of Nanoslot Antennas in Nonlinear Regime. Nano Lett 2015, **15**, 6683-8.

22. Yang, F.; Sambles, J. R. Resonant transmission of microwaves through a narrow metallic slit. Phys Rev Lett 2002, **89**, 063901.

23. Hibbins, A. P.; Sambles, J. R.; Lawrence, C. R.; Brown, J. R. Squeezing millimeter waves into microns. Phys Rev Lett 2004, **92**, 143904.

24. Lockyear, M. J.; Hibbins, A. P.; Sambles, J. R.; Lawrence, C. R. Microwave transmission through a single subwavelength annular aperture in a metal plate. Phys Rev Lett 2005, **94**, 193902.

25. Aydin, K.; Cakmak, A. O.; Sahin, L.; Li, Z.; Bilotti, F.; Vegni,

L.; Ozbay, E. Split-ring-resonator-coupled enhanced transmission through a single subwavelength aperture. Phys Rev Lett 2009, **102**, 013904.

26. Moon, T.; Lee, B.; Kim, T.-G.; Oh, J.; Noh, Y. W.; Nam, S.; Park, B. Microwave dielectric relaxation of the polycrystalline (Ba,Sr)TiO[sub 3] thin films. Applied Physics Letters 2005, 86, 182904.

27. Rosner, B. r. T.; van der Weide, D. W. High-frequency near-field microscopy. Review of Scientific Instruments 2002, **73**, 2505.

28. Jenkins, M. D.; Naether, U.; Ciria, M.; Sesé, J.; Atkinson, J.; Sánchez-Azqueta, C.; Barco, E. d.; Majer, J.; Zueco, D.; Luis, F. Nanoscale constrictions in superconducting coplanar waveguide resonators. Applied Physics Letters 2014, **105**, 162601.

29. Jeong, J.; Rhie, J.; Jeon, W.; Hwang, C. S.; Kim, D.-S. High-throughput fabrication of infinitely long 10 nm slit arrays for terahertz applications. Journal of Infrared, Millimeter, and Terahertz Waves 2014, **36**, 262-268.

30. Engen, G. F.; Hoer, C. A. Thru-Reflect-Line: An Improved Technique for Calibrating the Dual Six-Port Automatic Network Analyzer. IEEE Transactions on Microwave Theory and Techniques 1979, **27**, 987-993.

31. Colestock, P.; Foley, M. A generalized TRL algorithm for s-parameter de-embedding; United States, 1993-04-01, 1993.

32. Kyoung, J. S.; Seo, M. A.; Park, H. R.; Ahn, K. J.; Kim, D. S. Far field detection of terahertz near field enhancement of sub-wavelength slits using Kirchhoff integral formalism. Optics Communications 2010, **283**, 4907-4910.

33. Seo, M. A.; Park, H. R.; Koo, S. M.; Park, D. J.; Kang, J. H.; Suwal, O. K.; Choi, S. S.; Planken, P. C. M.; Park, G. S.; Park, N. K.; Park, Q. H.; Kim, D. S. Terahertz field enhancement by a metallic nano slit operating beyond the skin-depth limit. Nature Photonics 2009, **3**, 152-156.

34. Park, H. R.; Park, Y. M.; Kim, H. S.; Kyoung, J. S.; Seo, M. A.; Park, D. J.; Ahn, Y. H.; Ahn, K. J.; Kim, D. S. Terahertz nanoresonators: Giant field enhancement and ultrabroadband performance. Applied Physics Letters 2010, **96**, 121106.

35. Bahk, Y. M.; Park, H. R.; Ahn, K. J.; Kim, H. S.; Ahn, Y. H.; Kim, D. S.; Bravo-Abad, J.; Martin-Moreno, L.; Garcia-Vidal, F. J. Anomalous band formation in arrays of terahertz nanoresonators. Phys Rev Lett 2011, **106**, 013902.

36. Park, H.-R.; Bahk, Y.-M.; Ahn, K. J.; Park, Q. H.; Kim, D.-S.; Martín-Moreno, L.; García-Vidal, F. J.; Bravo-Abad, J. Controlling Terahertz Radiation with Nanoscale Metal Barriers Embedded in Nano Slot Antennas. ACS Nano 2011, **5**, 8340-8345.

37. Bahk, Y.-M.; Choi, J.-W.; Kyoung, J.; Park, H.-R.; Ahn, K. J.; Kim, D.-S. Selective enhanced resonances of two asymmetric terahertz nano resonators. Opt. Express 2012, **20**, 25644-25653.

38. Kang, J. H.; Choe, J.-H.; Kim, D. S.; Park, Q. H. Substrate effect on aperture resonances in a thin metal film. Opt. Express 2009, **17**, 15652-15658.

39. Park, H. R.; Koo, S. M.; Suwal, O. K.; Park, Y. M.; Kyoung, J. S.; Seo, M. A.; Choi, S. S.; Park, N. K.; Kim, D. S.; Ahn, K. J. Resonance behavior of single ultrathin slot antennas on finite dielectric substrates in terahertz regime. Applied Physics Letters 2010, **96**, 211109.

40. Levenson, M. D.; Viswanathan, N. S.; Simpson, R. A. Improving resolution in photolithography with a phase-shifting mask. IEEE Transactions on Electron Devices 1982, **29**, 1828-1836.

41. Switkes, M.; Rothschild, M. Immersion lithography at 157 nm. Journal of Vacuum Science & Technology B: Microelectronics and Nanometer Structures Processing, Measurement, and Phenomena 2001, **19**, 2353-2356.

42. Ghislain, L. P.; Elings, V. B.; Crozier, K. B.; Manalis, S. R.; Minne, S. C.; Wilder, K.; Kino, G. S.; Quate, C. F. Near-field photolithography with a solid immersion lens. Applied Physics Letters 1999, **74**, 501-503.

43. Finders, J.; Dusa, M.; Vleeming, B.; Hepp, B.; Maenhoudt, M.; Cheng, S.; Vandeweyer, T. Double patterning lithography for 32nm: critical dimensions uniformity and overlay control considerations.

MOEMS 2009, 8, 011002-011002-11.

44. Park, W.; Rhie, J.; Kim, N. Y.; Hong, S.; Kim, D.-S. Sub-10 nm feature chromium photomasks for contact lithography patterning of square metal ring arrays. Scientific Reports 2016, **6**, 23823.

45. Yin, L.; Vlasko-Vlasov, V. K.; Pearson, J.; Hiller, J. M.; Hua, J.; Welp, U.; Brown, D. E.; Kimball, C. W. Subwavelength Focusing and Guiding of Surface Plasmons. Nano Letters 2005, **5**, 1399-1402.

46. Novotny, L.; van Hulst, N. Antennas for light. Nature Photonics 2011, **5**, 83-90.

47. Lv, J.-T.; Yan, Y.; Zhang, W.-K.; Liu, Y.-H.; Jiang, Z.-Y.; Si, G.-Y. Plasmonic nanoantennae fabricated by focused Ion beam milling. International Journal of Precision Engineering and Manufacturing 2015, **16**, 851-855.

48. Yoo, D.; Nguyen, N. C.; Martin-Moreno, L.; Mohr, D. A.; Carretero-Palacios, S.; Shaver, J.; Peraire, J.; Ebbesen, T. W.; Oh, S. H. High-Throughput Fabrication of Resonant Metamaterials with Ultrasmall Coaxial Apertures via Atomic Layer Lithography. Nano Lett 2016, **16**, 2040-6.

49. Johnson, R. C.; Ecker, H. A.; Hollis, J. S. Determination of far-field antenna patterns from near-field measurements. Proceedings of the IEEE 1973, **61**, 1668-1694.

50. Yaghjian, A. An overview of near-field antenna measurements. IEEE Transactions on Antennas and Propagation 1986, **34**, 30-45.

51. Grischkowsky, D.; Keiding, S.; van Exter, M.; Fattinger, C. Far-infrared time-domain spectroscopy with terahertz beams of dielectrics and semiconductors. J. Opt. Soc. Am. B 1990, **7**, 2006-2015.

52. van Exter, M.; Fattinger, C.; Grischkowsky, D. Terahertz time-domain spectroscopy of water vapor. Opt. Lett. 1989, **14**, 1128-1130.

53. Wu, Q.; Litz, M.; Zhang, X. C. Broadband detection capability of ZnTe electro-optic field detectors. Applied Physics Letters 1996, **68**, 2924-2926.

54. Garcia-Vidal, F. J.; Moreno, E.; Porto, J. A.; Martin-Moreno, L. Transmission of light through a single rectangular hole. Phys Rev Lett 2005, **95**, 103901.

55. Kihm, H. W.; Koo, S. M.; Kim, Q. H.; Bao, K.; Kihm, J. E.; Bak, W. S.; Eah, S. H.; Lienau, C.; Kim, H.; Nordlander, P.; Halas, N. J.; Park, N. K.; Kim, D. S. Bethe-hole polarization analyser for the magnetic vector of light. Nat Commun 2011, **2**, 451.

56. Lee, D.; Kim, D. S. Light scattering of rectangular slot antennas: parallel magnetic vector vs perpendicular electric vector. Sci Rep 2016, **6**, 18935.

57. Seeger, K. Microwave dielectric constants of silicon, gallium

arsenide, and quartz. Journal of Applied Physics 1988, **63**, 5439-5443.

58. Bolivar, P. H.; Brucherseifer, M.; Rivas, J. G.; Gonzalo, R.; Ederra, I.; Reynolds, A. L.; Holker, M.; de Maagt, P. Measurement of the dielectric constant and loss tangent of high dielectric-constant materials at terahertz frequencies. IEEE Transactions on Microwave Theory and Techniques 2003, **51**, 1062-1066.

59. Lin, J.; Oh, S. H.; Nguyen, H. M.; Reitich, F. Field enhancement and saturation of millimeter waves inside a metallic nanogap. Opt Express 2014, **22**, 14402-10.

60. Gordon, R.; Brolo, A. G. Increased cut-off wavelength for a subwavelength hole in a real metal. Opt. Express 2005, **13**, 1933-1938.

61. Born, M. A. X.; Wolf, E. CHAPTER VII - ELEMENTS OF THE THEORY OF INTERFERENCE AND INTERFEROMETERS. In Principles of Optics (Sixth (Corrected) Edition), Wolf, M. B., Ed. Pergamon: 1980; pp 256-369.

62. Choi, S. B.; Park, D. J.; Jeong, Y. K.; Yun, Y. C.; Jeong, M. S.; Byeon, C. C.; Kang, J. H.; Park, Q. H.; Kim, D. S. Directional control of surface plasmon polariton waves propagating through an asymmetric Bragg resonator. Applied Physics Letters 2009, **94**, 063115.

63. Han, S.; Bahk, Y. M.; Park, N.; Kim, D. S. Terahertz field enhancement in asymmetric and tapered nano-gaps. Opt Express 2016, **24**, 2065-71.

64. Lee, J. W.; Seo, M. A.; Kang, D. H.; Khim, K. S.; Jeoung, S. C.; Kim, D. S. Terahertz electromagnetic wave transmission through random arrays of single rectangular holes and slits in thin metallic sheets. Phys Rev Lett 2007, **99**, 137401.

65. Park, H.-R.; Bahk, Y.-M.; Choe, J. H.; Han, S.; Choi, S. S.; Ahn, K. J.; Park, N.; Park, Q. H.; Kim, D.-S. Terahertz pinch harmonics enabled by single nano rods. Opt. Express 2011, **19**, 24775-24781.

66. Seo, M.; Kyoung, J.; Park, H.; Koo, S.; Kim, H. S.; Bernien, H.; Kim, B. J.; Choe, J. H.; Ahn, Y. H.; Kim, H. T.; Park, N.; Park, Q. H.; Ahn, K.; Kim, D. S. Active terahertz nanoantennas based on VO2 phase transition. Nano Lett 2010, **10**, 2064-8.

67. Jeong, Y.-G.; Paul, M. J.; Kim, S.-H.; Yee, K.-J.; Kim, D.-S.; Lee, Y.-S. Large enhancement of nonlinear terahertz absorption in intrinsic GaAs by plasmonic nano antennas. Applied Physics Letters 2013, **103**, 171109.

68. Choi, S. B.; Kyoung, J. S.; Kim, H. S.; Park, H. R.; Park, D. J.; Kim, B.-J.; Ahn, Y. H.; Rotermund, F.; Kim, H.-T.; Ahn, K. J.; Kim, D. S. Nanopattern enabled terahertz all-optical switching on vanadium dioxide thin film. Applied Physics Letters 2011, **98**, 071105.

국문초록

본 연구에서는 마이크로파 대역 실험을 통해 5 나노미터에 이르는 파장 이하 금속 틈에 의한 전기장 집속 현상을 관측하였다. 시료의 투과율과 전기장 집속도는 Ku band (12~18 GHz) 대역의 혼 안테나 쌍을 이용하여 측정하였다. 알루미늄 호일을 칼로 뚫어 파장보다 400배 작은 폭을 갖는 슬랏 안테나를 만들었으며 파장과 안테나 폭의 비율이 비슷한 테라헤르츠 대역 나노슬랏 안테나 연구들과 일치하는 결과를 얻었다. 보다 좁은 틈에서의 전기장 집속 현상을 확인하기 위해 원자층 리소그래피(atomic layer lithography)로 파장보다 10,000,000배 작은 틈을 갖는 나노갭 시료를 제작하였다. Ku, K (18~26.5 GHz), Ka (26.5~40 GHz) band 대역의 개방형 도파로 쌍을 제작했고 이를 이용해 5,000배에 이르는 전기장 집속을 확인하였다. 같은 시료를 테라헤르츠 시간영역 분광법으로 측정한 결과 또한 마이크로파 대역과 일치하였다. 파장보다 작은 틈에서의 전기장 집속의 응용분야로써, 부도체-금속 전이 현상을 기반으로 하는 마이크로파 스위치를 파장보다 2,000배 작은 폭을 갖는 슬랏 안테나 기반에서 구현하였다. 상기한 연구들은 마이크로파 및 밀리미터파 광학 소자의 비선형성과 민감도를 향상시킬 수 있으며 분자의 비파괴 포획과 빛에 의한 유체 제어를 가능하게 할 것이다.

키워드 : 마이크로파 투과(microwave transmission), 전자기장 집속(field enhancement), 파장한계광학(subwavelength optics), 나노갭(nanogap), 테라헤르츠 시간영역 분광법(terahertz time-domain spectroscopy)

학번 : 2012-30106

List of publications

1. **Kwanghee Lee**, Jeeyoon Jeong, Young-Mi Bahk, Jiyeah Rhie, In-Keun Baek, Bong Jun Lee, Yu Hyun Kang, Seunghun Hong, Gun-Sik Park, and Dai-Sik Kim, Microwave Funneling through Sub-10 nm Nanogaps, *ACS Photonics* **3**, 537 (2016)

2. **Kwanghee Lee**, *et al*., Deep subwavelength optics with λ/400-wide hand-made metallic gaps. (in preparation)

Conferences

1. (Poster) Experimental Study of Microwave Resonances for λ/400 Slot Antennas, **Kwang-Hee Lee**, Young-Mi Bahk, and Dai-Sik Kim, **Asia-Pacific Microwave Photonics Conference 2013**, Gwangju, Korea, 22-24 April, 2013

2. (Oral) Experimental study of microwave resonances for λ/400 slot antennas, **Kwang-Hee Lee,** Young-Mi Bahk and Dai-Sik Kim, **KPS**, Daejeon, Korea, 24-26 April, 2013

3. (Oral) Resonance properties of asymmetric slot antenna pairs in deep subwavelength regime, **Kwanghee Lee,** Young-Mi Bahk, Jeeyoon Jeong, and Dai-Sik Kim, **Optical Society of Korea Summer Meeting 2013**, Yeosu, Korea, 10-12 July, 2013

4. (Oral) Huge field enhancement in microwave range achieved by λ/2000-width antennas, **Kwanghee Lee**, Jiyeah Rhie, Young-Mi Bahk, Jeeyoon Jeong, and Dai-Sik Kim, **IRMMW-THz 2014**, Tucson, AZ, USA, 14-19 September, 2014

5. (Poster) Electric field enhancement in few nanometer-width antennas operating at gigahertz range, **Kwanghee Lee**, Jeeyoon Jeong, Jiyeah Rhie, and Dai-Sik Kim, **META15**, New York, USA, 4-7 August, 2015

6. (Oral) Electromagnetic Wave Funneling Through λ/10,000,000 Nanogaps For Microwave Regime, **Kwanghee Lee**, Jeeyoon Jeong, Jiyeah Rhie, Young-Mi Bahk, and Dai-Sik Kim, **IRMMW-THz 2015**, Hong Kong, 23-28 August, 2015

7. (Oral) Microwave and Millimeter-wave Funneling through Nanogaps, **Kwanghee Lee**, Jeeyoon Jeong, Young-Mi Bahk, Jiyeah Rhie, In-Keun Baek, Seunghun Hong, Gun-Sik Park, and Dai-Sik Kim, **KPS**, Kwangju, Korea, 19-21 October, 2016